Imperial College London

Transition In Stratified Shear Flows:
Linear Stability Analysis With A Shear And Stratification Unalignment
Final Year Project

Academic Supervisor: Dr. Yongyun Hwang
Academic Second Marker: Prof. Sergei Chernyshenko
Department: Aeronautics
Academic year: 2019/2020

Student: Joel Outschoorn
Date: May 26, 2020

Abstract

Linear Stability Analysis of a density stratified shear flow, where the stratification is unaligned to the shear, is presented here. This project aims to unlock a more complete understanding of the consequences of tilting the stratified plane to the shear plane and identify the conditions which induce a destabilisation effect. The study shall be limited to the plane Couette (pCf) and plane Poiseuille flow (pPf) where the shear is tilted with respect to the stratification by angle θ. A stratified Orr-Sommerfeld and Squire system was derived and the Chebyshev Transform Method was utilised to develop a Stratified Solver, using MATLAB, which solved the problem of unaligned stratified shear stability. The main findings were that destabilisation due to the unalignment begins at $\theta = 50$ degrees. The induced instability is found at wavenumbers $(\alpha, \beta) = (0.8, 5)$ and $(\alpha, \beta) = (1.5, 6)$ for the pCf and pPf respectively. As θ is increased from 0 to 90 degrees, there is an apparent exponential decay in the transitional Reynolds number, Re_{crit}, as the flow destabilises. For the pCf, the most unstable eigenmode begins as a conjugate pair and as θ is raised, the pair moves closer together, with a reduction in the oscillatory frequency. Between an angle of 60 to 80 degrees, the two eigenmodes coalesce into a single purely non-oscillatory unstable mode. As for the Froude number, F_h, when unaligned, increasing the stratification strength had a stabilising effect until a critical Froude number, $F_{h,crit}$, below which strengthening the stratification has a destablising effect; for the pCf, $F_{h,crit} \approx 1$. Further evaluation of Re and the perturbed profiles concluded that the instability was dictated by an inviscid mechanism and involved the resonance of two Doppler shifted waves.

Contents

Acknowledgements

A handful of academics played a vital role in my completion of this project, firstly and most importantly, I want to express my gratitude to Dr. Yongyun Hwang for his complete supervision throughout this year, and I must mention Professor Sergei Chernyshenko for his feedback at the Interim Assessment. I would also like to thank my academic tutor, Dr. Thulasi Mylvaganam for her unconditional guidance and care during my time at Imperial College.

List of Figures

List of Tables

Nomenclature

Acronyms

DNS	Direct Numeric Simulation	
HSA	Hydrodynamic Stability Analysis	
ISA	International Standard Atmosphere	
LSA	Linear Stability Analysis	
pBj	Plane Bickley jet	
pCf	Plane Couette flow	
pPf	Plane Poiseuille flow	

Important Non-Dimensional Parameters

Re	Reynolds number	$\frac{UL}{\nu}$
Re_{crit}	Transitional Reynolds number	$\frac{UL}{\nu}$
F_h	Horizontal Froude number	$\frac{U}{NL_h}$
F_v	Vertical Froude number	$\frac{V}{NL_v}$
Ri	Bulk Richardson number	F_h^{-1}
Sc	Schmid number	$\frac{\nu}{K}$
b	Dimensionless buoyancy	$\frac{\rho' g}{\rho_0}$
α	x-direction wavenumber	-
β	z-direction wavenumber	-
k^2	Constant parameter	$\alpha^2 + \beta^2$

List of Symbols

ρ	Fluid density	$\mathrm{kg/m^3}$
ρ_0	Reference fluid density	$\mathrm{kg/m^3}$
U	Fluid mean velocity	m/s

N_{BV}	Brunt–Väisälä frequency	s^{-1}
L	Characteristic length	m
t	Characteristic time scale	s
∇	Vector differential operator	-
p	Pressure	Pa
ν	Kinematic viscosity	m^2/s
g	Gravitational acceleration	m/s^2
K	Mass diffusivity	m^2/s
$U(y)$	Fully developed velocity profile	m/s
θ	Shear plane tilt angle with respect to stratification plane	degrees
$\mathbf{u}$	Velocity vector (u, v, w) in the (x, y, z) directions	m/s
η	Wall-normal vorticity	s^{-1}
$\mathcal{L}$	Linear Stability Analysis matrix coefficient	-
i	Imaginary number; $\sqrt{-1}$	-
a_n	Chebyshev coefficient	-
$T_n(x)$	Chebyshev polynomial of order n	-
ω	Complex frequency	$\omega_r + i\omega_i$
ω_r	Oscillatory frequency	-
ω_i	Growth rate	-
$\omega_{i,0}$	Most stable growth rate	-
$\omega_{i,max}$	Most unstable growth rate	-
(x, y, z)	Shear plane	-
(X, Y, Z)	Stratification plane	-
$\mathcal{D}$	Derivative with respect to y	-
N	Number of Chebyshev grid points	-
$flow$	Stratified MATLAB Solver input parameter for the chosen shear flow	-
$plotFigure$	Stratified MATLAB Solver input parameter for user request to plot figures	-

Chapter 1

Introduction

Shear and density stratification are common features of Earth flow fields. Stratified shear flows are fluids that have significant velocity and density gradients. While typical aeronautical practices might not encounter these flows, they are ubiquitous in other applications, such as oceanography, meteorology and industrial flows. In the ocean, due to gravitational influences, the fluid is more saturated with salts at lower depths which creates a density stratified fluid. As for the atmosphere, it is known that the air exhibits a density gradient, again due to gravity,. The International Standard Atmosphere (ISA) models the stratification by splitting the atmosphere into layers, each with its own density gradient. Stratification modifies shear stability characteristics and flow evolution behaviours following disturbances thus making it an area of interest.

1.1 Motivations

Shear instability is one of the famous fields of research in fluid dynamics. The evolution of shear flows has been broadly studied due to its industrial and geophysical interest. However, research in the effects of an applied uniform density stratification on the linear growth of shear instability is still absent. The influence of stable stratification is widely agreed to be stabilising in the case of shear and stratified alignment. Likewise, the study of orthogonality of these two gradient profiles has been extensively investigated, mainly from Facchini [1] and Lucas [3] where a streamwise shear has an applied stable spanwise linear stratification. In the analysis presented here, the examination of a stratified plane shear flow is carried out for the scenario where the shear and stratification are not aligned, which is typical of industrial flows. The transition of these stratified structures to turbulence has not been well understood. The fundamental interest of this project will be to study the early stage of transition in unaligned stratified shear flows using linear dynamical systems theory.

The density variations strongly influence the fluid dynamics particularly the stability of such flows. Important parameters which quantify stratified fluids are the Brunt–Väisälä frequency, N_{BV}, and the Froude number, F_h. These constants determine the strength of the density stratification and their significance will be discussed in Chapter 3. The shear flows that were investigated were mainly the plane Couette flow (pCf), Figure 1.1(a), and plane Poiseuille flow (pPf), Figure 1.1(b). pCf arises from two plates moving in opposite directions which creates a linear velocity gradient, whereas pPf are formed by a downstream pressure drop with non-moving plates and the fully developed flow structure would give rise to a parabolic velocity profile. The flow structures that will be investigated is a plane shear flow that is tilted by an unalignment angle, θ, with respect to a linear density gradient plane produced by a gravity vector g, which is visualised in Figure 1.1.

To illustrate the various findings, this report is organised as follows. Chapters 2 and 3 provides a breakdown of the fundamental theories that will be applied, with Chapter 2 summarising the fluid dynamic analysis and Chapter 3 will focus on understanding stratified flows. Chapter 4 presents the main goals of the project. Chapter 5 provides the formulation of the governing system of equations and defines the various parameters of interest. Chapter 6 presents the numerical method that was implemented and analysis on the reliability of the chosen method. Chapter 7 provides the main results and discussions from the analysis and finally Chapter 8 considers potential further studies and the main conclusions.

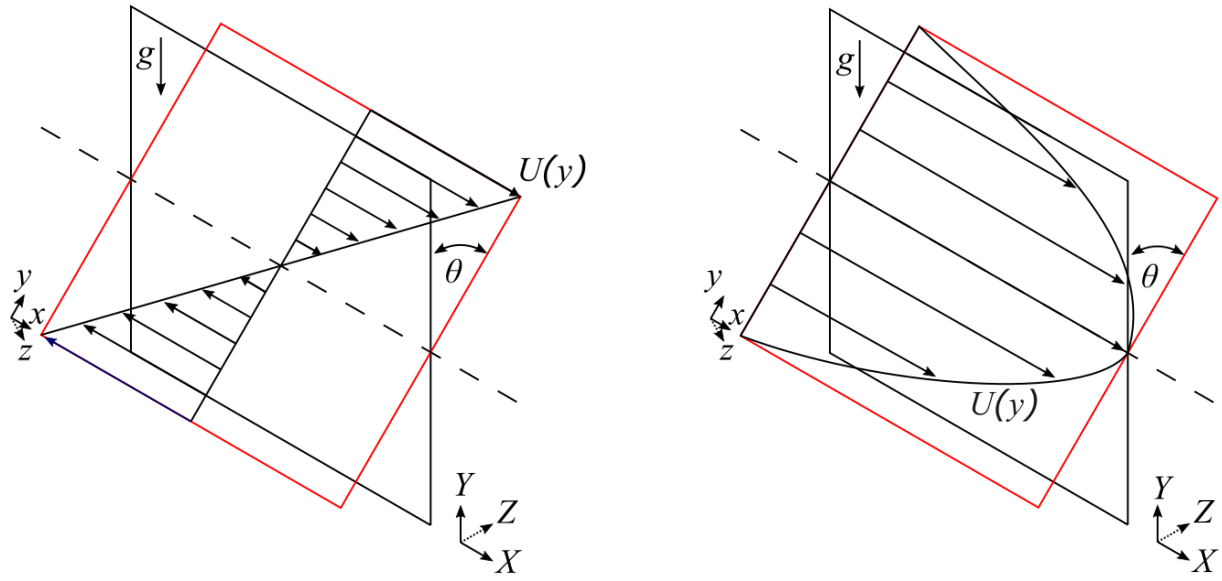

(a) Plane Couette flow (pCf).

(b) Plane Poiseuille flow (pPf).

Figure 1.1: Shear plane (x, y, z), in red, tilted with respect to the stratification plane (X, Y, Z) by angle θ in degrees.

Chapter 2

Literature Review: Hydrodynamic Stability

This chapter endeavours to demonstrate a brief introduction on the theories of Linear Stability Analysis (LSA), a field of Hydrodynamic Stability Analysis, for parallel shear flows. The information for LSA was largely provided through [4].

Hydrodynamic Stability Analysis (HSA) is the branch of fluid dynamics investigating the transition of laminar flows to turbulence structures. Transition is sensitive to external noise and disturbances leading to dramatic changes in the flow field. The governing equations of fluid dynamics (in the unstratified case would be the Navier Stokes equations) produces basic laminar flow structures as a basic solution. In some cases, these laminar states are prone to instabilities due to certain critical conditions. The unstable modes causes the flow to evolve into more complicated flow patterned/unpatterned (turbulent) states. The study of HSA is important mainly because it provides an explanation as to the discrepancy between analytical solutions that satisfy the governing equation and what is naturally occurring or observable in experiments.

HSA allows fluid structures to be modelled as a system, with the known solution in the space-time field as the basic equilibrium flow. When the system is deviated from this equilibrium state, the system stability characterises whether the flow arrangement will return to its original basic flow or whether the flow field will break down into turbulent structures. The formal definition of stability is in the Lyapunov sense, however we will assume the perturbations are infinitesimal. It must be pointed out that nonlinear or secondary instabilities do hold significance to destabilise flows. Nevertheless, previous work has proven that primary linear stability first govern the flow behaviour before any global or non-linear stability.

The main analysis that shall be presented in this report is fundamentally the solutions to an eigenvalue problem, where the eigenspectra determines the base flow stability and the eigenfunctions give the shape of the state perturbations.

2.1 Linear Stability Analysis

LSA is a branch of HSA which investigates the initial onset of these instabilities and the critical conditions which induces them. The dynamics of perturbations from a fully developed equilibrium base flow is examined. The instability is caused if these perturbations were to exhibit signs of temporal growth. The mathematical definition for stability is the supression of these perturbations.

The linear stability considered here will be referenced from two-dimensional parallel shear flows and shall follow the fundamental steps of famous Orr-Sommerfeld/Squire system of equations which governs the stability of uni-directional viscous fluids.

The main steps of LSA are presented below:

- Introduce the base flow velocity profile, in our case is the pCf and pPf profiles. Decompose the profile into an equilibrium flow and a perturbation state.
- Substitute this decomposed velocity profile into the governing equations of motion. Apply linearisation by neglecting higher order terms; squared and above $\mathcal{O}(\epsilon^2) \to 0$.
- Next develop a normal mode solution which will be of an exponential form with the spatial and temporal terms. Substitute this solution into the linearised governing equations.
- Following certain manipulations for the Orr-Sommerfeld/Squire equations reduce the governing equations into a finalised eigenvalue system.

The formulation of the stratified eigenvalue problem is presented in Chapter 5 and, for clarity, the complete derivation is illustrated in Appendix A.

2.1.1 Introduction To Absolute and Convective Instability

A brief discussion of the significance of the types of linear instabilities typically found is introduced here. Considering the linear stability of an open flow, if all infinitesimal perturbations decay over a domain in time and space, the flow is linearly stable. Many flows are open flows, hence disturbances and external excitations can be washed downstream hence the flow should always be stable, granted there is no continuous perturbation. This notion led to the definitions of absolute and convective instabilities. These distinguish between perturbation stabilities that would be convected away or those that would remain and grow. The formal definitions for Convective and Absolute Instabilities are:

- Linearly Convectively Unstable: Disturbances that grow in space and time but are ultimately advected away from the region of interest by the freestream.
- Linearly Absolutely Unstable: Disturbances that grow in space and time but remain at the source.

Absolute and convective instabilities are identified mathematically through examination of the computed eigenspectra from performing LSA. In this case, the eigenspectra physically represent the complex frequency parameter, $\omega = \omega_r + i\omega_i = \text{Real}(\omega) + i\text{Imag}(\omega)$, where as shown $\omega \in \mathbb{C}$, which will be defined and discussed in Section 5. The stability criterion, defined in [4], depends on the imaginary part of ω, which physically represents the perturbation growth rate, ω_i. Generally linear instability is found when $\omega_i > 0$. As for determining absolute and convective instabilities requires a closer look at each eigenmode of the spectrum as shown in Table 2.1.

Table 2.1: Mathematical criterion for absolute and convective instabilities depending on the growth rate of the eigenspectra. Note that +ve and -ve represent positive and negative growth rates respectively.

$\omega_{i,0}$	$\omega_{i,max}$	Absolute	Convective
-ve	-ve	Stable	Stable
-ve	+ve	Stable	Unstable
+ve	+ve	Unstable	Unstable

Note that ω_i is sorted in terms of increasing stability, and $\omega_{i,max}$ represents the most unstable eigenmode and $\omega_{i,0}$ represents the most stable eigenmode. Qualitivately, each eigenmode represents a local region of the flow field. Hence, the conditions stated above represent the cases when only some regions of the flow is prone to instability, this is defined as being convectively unstable. However, the case when all regions of the flow is unstable, the flow is absolutely unstable. The analysis in this project does not concern itself too much on the types of instabilities occurring but more the conditions that induce instabilities and the influence of the tilt on the base flow transitional behaviour, hence the analysis shall be looking at the onset of $\omega_{i,max} > 0$. Future developments of the works of this project may look into the types of instabilities occurring at critical conditions and further look into how the tilts affects each of these instabilities.

Chapter 3

Literature Review: Stratified Flows

This Chapter aims to introduce the concept of stratification and review the main findings of stability analysis carried out by past researchers into the transition of stratified shear flows, mainly concerning the pCf and plane Bickley jet (pBj). These literature provided the validation means for the developed numerical solver. Stratified shear flows are simply fluids with a density variation. Therefore, there exists a density profile as well as the shear velocity profile. Means to quantify stratified fluids is described in Section 3.1, while their governing system of equations will be discussed in Section 3.2. Past works on stratified flows are reviewed in Sections 3.3 and 3.4, where Section 3.4 looks into previous works of tilted stratified shear flows.

3.1 Non-Dimensional Parameters

Stratification is quantified using the Brunt–Väisälä frequency, N_{BV}, where increasing this parameter strengthens the density gradient. The Froude number, F, and the bulk Richardson number, Ri, are dimensionless parameters defining the density gradient strength, where $Ri = F_h^{-1}$.

$$F = \frac{u}{NL} \tag{3.1.1}$$

The Froude number, determined by Equation (3.1.1), is more typically used in existing research, where u is the flow velocity and L is the characteristic length. It quantifies the stratification strength based from the Brunt-Vaisala frequency. For two-dimensional flows, one can define F both in the horizontal, F_h, and vertical, F_v, direction using the velocities (U, V) and lengths (L_h, L_v) representing the horizontal and vertical directions. Since this project works with parallel base flows, only $F_h = (\frac{U}{NL_h})$ is considered. The criteria for strongly stratified flows are those with $F_h \leq 1$, with stronger density gradients achieved by reducing F_h.

3.2 Governing Equations

The governing equations that model stratified fluids are the Navier-Stokes equations under the Boussinesq approximation [5]. Here a linear stratification is applied to the momentum equations via a gravity gradient acting downwards. Therefore, the density decreases linearly as you move up the vertical direction. The Boussinesq approximation also models the density transport, however these density variations are assumed to be small. Hence, an incompressible flow assumption is still valid. The governing system is shown in Equations (3.2.1) to (3.2.3) below:

$$\frac{\partial \mathbf{u}^*}{\partial t^*} + (\mathbf{u}^* \cdot \nabla)\mathbf{u}^* = -\frac{\nabla p^*}{\rho_0^*} + \nu^* \nabla^2 \mathbf{u}^* - \frac{\rho'^* g^*}{\rho_0^*}\hat{\mathbf{Y}} \tag{3.2.1}$$

$$\frac{\partial u^*}{\partial x^*} + \frac{\partial v^*}{\partial y^*} + \frac{\partial w^*}{\partial z^*} = 0 \tag{3.2.2}$$

$$\frac{\partial \rho'^*}{\partial t^*} + (\mathbf{u}^* \cdot \nabla)\rho'^* = K^* \nabla^2 \rho'^* \tag{3.2.3}$$

Equations (3.2.1) represent the momentum terms where $\mathbf{u} = (u, v, w))$ is the three-dimensional velocity vector, p is the pressure state, ν the kinematic viscosity, ρ' and ρ_0 are the density perturbation and reference density respectively and g is the gravity which provides the stratification. $\hat{\mathbf{Y}}$ simply represents the direction of the density gradient. Equation (3.2.2) illustrates the continuity equation, where an incompressible assumption has already been applied. Finally, Equation (3.2.3) presents the density transport given from the Boussinesq approximation, where K is the density diffusivity. Note that the (*) represents dimenioned variables. It is useful to non-dimensionalise these equations in order to reduce error. The use and manipulation of these equations will be illustrated in Chapter 5.

3.3 Past Work On Stratified Shear Flow Stability

Initially, to understand the notion of stratified flows, [6], was reviewed. The main points were conveying the idea that strongly stratified fluids would arrange itself into layered structures with density interfaces. This paper mainly discussed the manipulations to the governing equations to provide dimensionless forms and the significance of the domain sizes of the control volume.

There has been a considerable amount of work on the stability of stratified shear flows with spanwise stratification (shear and stratified orthogonality). The general configuration of these flow structures is shown in Figure 3.1. Lucas [3] investigates the effect of stable spanwise stratification on the pCf. The main results showed how turbulent flows illustrate near-wall layering. Moreover, when N_{BV} suppresses turbulence, the linear instabilities lead to ordered nonlinear states with the possibility of secondary shear instablities. The three-dimensional stability of spanwise stratified shear flows was investigated in Deloncle [7]. Here, they found that the Squire theorem, where the most unstable perturbation in homogeneous fluids is always two-dimensional, does not apply for stably stratified fluids. They found that the stronger the stratification, the smaller the vertical scales that can be destabilised.

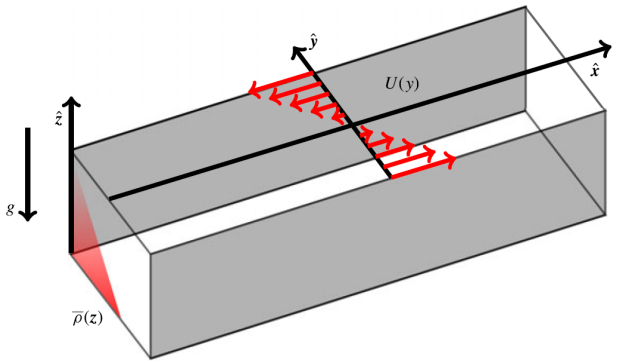

Figure 3.1: Sketch of spanwise stratified pCf from [1]. $U(y)$ and $\bar{\rho}(z)$ represents the velocity and density profile (produced by gravity g) respectively. ($\hat{\mathbf{x}}$,$\hat{\mathbf{y}}$,$\hat{\mathbf{z}}$) are directions: streamwise, stream-normal and spanwise.

Facchini [1] provided the means of validation for the developed LSA Solver. Facchini presents the analysis of the pCf with orthogonal stratification. They performed LSA on the described fluid structure, along with non-linear Direct Numeric Simulations (DNS) and experimental data for validation. The stability was characterised by the Reynolds number, Re and F_h. The main result was that the flow becomes unstable for moderate values of $Re \geq 700$ and for $F_h \approx 1$. The instability is induced from a wave resonant mechanism, known in channel flows.

3.4 Past Work On Shear Stratification Unalignment

Candelier [2] carried out analysis on a tilt angle between the stratification and shear. The analysis was on a two-dimensional pBj with a gravity-induced stratification plane as shown in Figure 3.2. For the aligned case, the condition for stability is based on $Ri \geq 1/4$. However, in the unaligned case, the pBj is found to always be unstable for all F_h. The fundamental result was that aligning stratification with shear provides stabilisation. This is a known result, as the stratification inhibits vertical growth of perturbations from the density gradient, hence the flow relaminarises following deviations. Once unaligned, this induces shear flow instabilities.

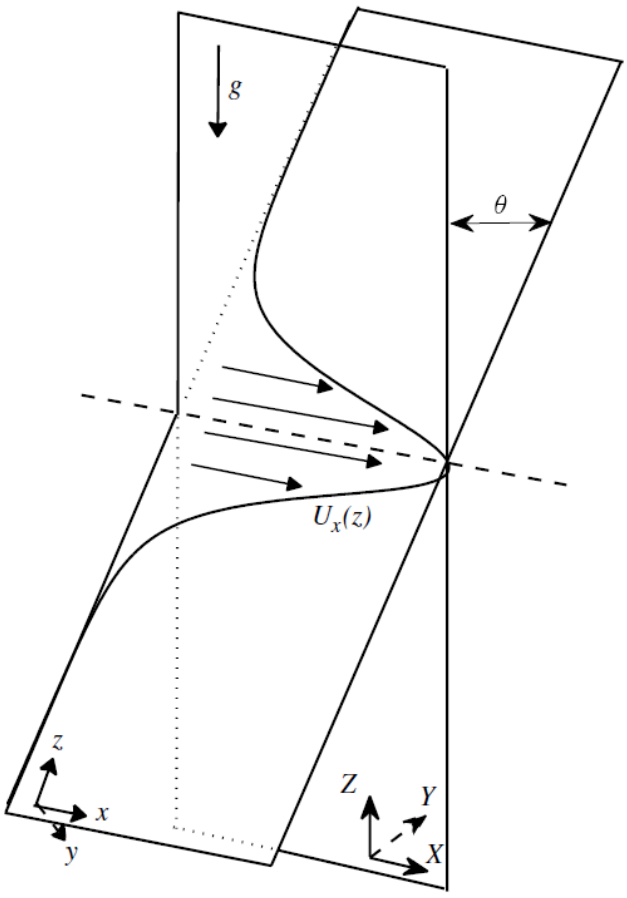

Figure 3.2: Sketch of the base flow (pBj) unaligned to the stratification plane (provided by g) by angle θ from [2]. $U_x(z)$ is the shear velocity profile and there are two coordinate systems where (x, y, z) is the shear plane and (X, Y, Z) is the stratification plane.

Chapter 4

Project Aims and Assumptions

The fundamental goal in a larger context is working towards to a complete understanding of density stratification with a tilted plane shear flow. In the examined work, we look to study the effect of this inclination angle on the linear properties of the shear instability. This project does not mean to achieve a finalised picture of the flow physics but is the first steps towards a thorough and clear-cut understanding. Future work will be required to build on the outcomes of this project to build towards a complete understanding and as stated earlier we shall limit ourselves to linear analysis.

4.1 Assumptions and Approximations

The basis of the presented work will be on linear stability analysis as we concern ourselves with the onset of exponential growth of perturbations from a fully developed base flow. Linear stability analysis first governs the local absolute instability before transitioning to patterned or turbulent structures. From calculation of the onset of instabilities, one should be able to recreate trends similar to experimental observation. The fundamentals of LSA requires us decouple our state parameters into an equilibrium profile plus a perturbation term. Our concern is with the evolution of this perturbation term and to investigate the particular conditions that may suppress or destabilise these deviations from the laminar base flow.

The main assumptions that shall be implemented is a fully developed parallel base flow with only a velocity gradient in the vertical direction, U(y). Hence, the base flow will be a two-dimensional plane fluid structure. The stratified plane will be derived from a gravitational force which will produce a linear density gradient. The tilted shear flow will produce three-dimensional turbulent structures. Furthermore, the common assumptions of no-slip shear plane boundaries and impenetrable walls are implicitly implied in the project. Despite working with a density gradient, the density transport in the streamwise direction is assumed to be infinitesimal, hence we shall incorporate an incompressible fluid assumption. As a typical application of stratified flows is within oceans, this is a valid assumption.

4.2 Aims and Objections

The presented work aims to provide a more quantitative and theoretical understanding on the effect of unaligned stratification to shear flow stability and the threshold conditions to which the flow remains stable. In particularly,, it is well known that, in the unstratified case, the pCf is always linearly stable and the pPf has a critical Re of 5772 [8]. Hence, the influence of introducing a density gradient will be examined in comparison to the unstratified and the aligned stratification cases. Likewise, observation of the destabilising mode that happens at high stratification when they are not aligned is of interest.

Chapter 5

Theoretical Framework

This chapter formulates the stratified system of equations that will be solved by LSA, starting from the governing equations with the Boussinesq approximation that was introduced in Section 3.2. The derivation largely follows the steps of the famous Orr-Sommerfeld/Squire system for parallel shear flows as presented in [4]. The stratified fluid structure was introduced in Figure 1.1, showing both investigated shear flows.

5.1 Formulation

The pCf base flow is generated by two parallel moving walls with opposite velocities, while the pPf base flow is generated by a downstream pressure gradient with non-moving no-slip walls which generates the parabolic profile. The shear flow is tilted to the stratification plane by angle θ.

5.1.1 Coordinate System

Figure 1.1 visualises the flow structure this project concerns itself with. Observing the Figure, the initial laminar shear flow is assumed to be two-dimensional, where the shear plane is confined to the $(\hat{\mathbf{x}}, \hat{\mathbf{y}}, \hat{\mathbf{z}})$ coordinate system and the stratification plane is confined to $(\hat{\mathbf{X}}, \hat{\mathbf{Y}}, \hat{\mathbf{Z}})$. We use the $(\hat{\cdot})$ symbol to define unit vectors in the respective direction. We denote $\hat{\mathbf{x}}$ as the streamwise direction, $\hat{\mathbf{y}}$ as the stream-normal direction and $\hat{\mathbf{z}}$ as the spanwise direction. The variable g denotes gravity, which has vector $\mathbf{g} = (0\hat{\mathbf{X}} - g\hat{\mathbf{Y}} + 0\hat{\mathbf{Z}})$, while the arrows shape the constant shear velocity profile, which only changes in the stream-normal direction, $U(y)$. The tilt angle θ is with respect to the centre of each plane, where the shear plane is unaligned to the stratification plane. This tilt angle gives the transformations between coordinate systems as:

$$(\hat{\mathbf{X}}, \hat{\mathbf{Y}}, \hat{\mathbf{Z}}) = (\hat{\mathbf{x}}, \hat{\mathbf{y}}\cos\theta - \hat{\mathbf{z}}\sin\theta, \hat{\mathbf{y}}\sin\theta + \hat{\mathbf{z}}\cos\theta) \tag{5.1.1}$$

5.1.2 Governing Equations

For clarity, we reintroduce our system of equations under the Boussinesq approximation, where (*) represents dimensioned variables:

$$\frac{\partial \mathbf{u}^*}{\partial t^*} + (\mathbf{u}^* \cdot \nabla)\mathbf{u}^* = -\frac{\nabla p^*}{\rho_0^*} + \nu^* \nabla^2 \mathbf{u}^* - \frac{\rho'^* g^*}{\rho_0^*}\hat{\mathbf{Y}} \tag{5.1.2}$$

$$\frac{\partial u^*}{\partial x^*} + \frac{\partial v^*}{\partial y^*} + \frac{\partial w^*}{\partial z^*} = 0 \tag{5.1.3}$$

$$\frac{\partial \rho'^*}{\partial t^*} + (\mathbf{u}^* \cdot \nabla)\rho'^* = K^* \nabla^2 \rho'^* \tag{5.1.4}$$

5.1.3 Non-dimensionalisation

For convenience, one should look to non-dimensionalise the governing equations. This can be done in many ways as analysed by Billant [6]. The most intuitive way to non-dimensionalise is the use of the time-average mean velocity, characteristic length and reference density. This allows us to introduce the important dimensionless parameters; Reynolds number Re, Schmid number Sc and the previously defined F_h. Re allows the parameterisation of the viscosity strength. A higher Re represents a more inviscid flow. Sc is defined as the ratio of momentum diffusivity (ν) and mass diffusivity K, and is used to characterise fluid flows in which there are simultaneous momentum and mass diffusion convection processes. Next we can also introduce the dimensionless buoyancy $b = \frac{\rho' g}{\rho_0}$.

$$\frac{\partial \mathbf{u}}{\partial t} + (\mathbf{u} \cdot \nabla)\mathbf{u} = -\nabla p + \frac{1}{Re}\nabla^2 \mathbf{u} - \frac{b}{F_h^2}\hat{\mathbf{Y}} \tag{5.1.5a}$$

$$\frac{\partial \mathbf{u}}{\partial t} + (\mathbf{u} \cdot \nabla)\mathbf{u} = -\nabla p + \frac{1}{Re}\nabla^2 \mathbf{u} - \frac{b}{F_h^2}(\cos\theta \hat{\mathbf{y}} - \sin\theta \hat{\mathbf{z}}) \tag{5.1.5b}$$

$$\frac{\partial u}{\partial x} + \frac{\partial v}{\partial y} + \frac{\partial w}{\partial z} = 0 \tag{5.1.6}$$

$$\frac{\partial b}{\partial t} + (\mathbf{u} \cdot \nabla)b = \frac{1}{ReSc}\nabla^2 b \tag{5.1.7}$$

Equations (5.1.5) to (5.1.7) represent the dimensionless version of our original dimensioned system of Equations (5.1.2) to (5.1.4). Note that the momentum Equation (5.1.5a) has the buoyancy applied in the stratification plane, therefore by using (5.1.1), the momentum equation system can be rewritten as (5.1.5b). A key thing to note is that our density transport equation is now in terms of the dimensionless buoyancy, as shown in (5.1.7). Equation (5.1.6) remains as the dimensionless continuity expression that already has the incompressiblity applied to it.

Equations (5.1.5) to (5.1.7) will be taken forward as the systems governing equation system and the derivation of the eigenvalue problem will follow from these equations. The next step is to decouple the equation states $(\mathbf{u}, p, b)$ into a basic solution, $(\mathbf{u}_0, p_0, b_0)$, plus a perturbation term, $(\mathbf{u}', p', b')$. This is shown in Equation (5.1.8). Note that the basic solution for the velocity state is $\mathbf{u}_0 = (U(y), 0, 0)$ with perturbed velocities (u', v', w').

$$\begin{aligned} \mathbf{u} &= \mathbf{u}_0 + \mathbf{u}' \\ p &= p_0 + p' \\ b &= b_0 + b' \end{aligned} \tag{5.1.8}$$

5.1.4 Linearisation

These state solutions are then subbed into the dimensionless governing equations. The perturbed terms are assumed to be infinitesimally small, hence any second order terms and higher are approximated as

negligible giving the linearised governing equations presented below.

$$\frac{\partial u'}{\partial t} + U\frac{\partial u'}{\partial x} + v'\frac{dU}{dy} = -\frac{\partial p'}{\partial x} + \frac{1}{Re}\nabla^2 u' \tag{5.1.9a}$$

$$\frac{\partial v'}{\partial t} + U\frac{\partial v'}{\partial x} = -\frac{\partial p'}{\partial y} + \frac{1}{Re}\nabla^2 v' - \frac{b'}{F_h^2}\cos\theta \tag{5.1.9b}$$

$$\frac{\partial w'}{\partial t} + U\frac{\partial w'}{\partial x} = -\frac{\partial p'}{\partial z} + \frac{1}{Re}\nabla^2 w' + \frac{b'}{F_h^2}\sin\theta \tag{5.1.9c}$$

$$\frac{\partial u'}{\partial x} + \frac{\partial v'}{\partial y} + \frac{\partial w'}{\partial z} = 0 \tag{5.1.10}$$

$$\frac{\partial b'}{\partial t} + U\frac{\partial b'}{\partial x} - (\mathbf{u}'\cdot\nabla)\left(\frac{Y}{F_h^2}\right) = \frac{1}{ReSc}\nabla^2 b' \tag{5.1.11}$$

Equation (5.1.9) illustrates the linearised momentum equations, expressing all the (x, y, z) components and Equation (5.1.10) gives the linearised incompressible continuity expression. The linearised density transport equation, Equation (5.1.11), was derived with the help of Hwang and Fung [9]. The Y term is the vertical direction in the stratification plane. To transform the equation into the shear plane, one must use Equation (5.1.1).

5.2 Normal-Mode Solution

The state variables are (u', v', w', p', b'). However, this would create a large system that would have a heavy computational cost. Following the Orr-Sommerfeld/Squire system, we can introduce the wall-normal voriticity, expressed by Equation (5.2.1) below:

$$\eta' = \left(\frac{\partial u'}{\partial z} - \frac{\partial w'}{\partial x}\right) \tag{5.2.1}$$

Hence, some manipulation is required in order to reduce the system to state variables (v', η', b'). Local stability properties are then obtained by considering the perturbed states as a plane wave with the normal mode solution shown in Equation (5.2.2):

$$(v', \eta', b') = (\tilde{v}, \tilde{\eta}, \tilde{b})\exp(i(\alpha x + \beta z - \omega t)) \tag{5.2.2}$$

where α and β are the input wavenumbers in the streamwise and spanwise directions ($(\alpha, \beta) \in \mathbb{R}$) and $\omega = \omega_r + i\omega_i$ is the previously mentioned complex frequency. The real part of ω is the oscillation frequency of the eigenmode and the imaginary part is the growth rate. ω_i is the significant variable of interest. It determines the local stability of the perturbed state. $(\tilde{v}, \tilde{\eta}, \tilde{b})$ are the eigenfunctions that give the perturbed state variable shapes and ω gives the eigenspectra.

With the normal mode solution one can then substitute out the partial derivatives in the velocity, vorticity and density forms to assemble the final eigenvalue system. These substitutions are shown below:

$$\frac{\partial}{\partial t} = -i\omega, \quad \frac{\partial}{\partial x} = i\alpha, \quad \frac{\partial}{\partial y} = \mathcal{D}, \quad \frac{\partial}{\partial z} = i\beta; \quad \frac{\partial^2}{\partial x^2} = -\alpha^2, \quad \frac{\partial^2}{\partial y^2} = \mathcal{D}^2, \quad \frac{\partial^2}{\partial z^2} = -\beta^2$$

As in commonly implemented in HSA, the constant $k^2 = \alpha^2 + \beta^2$ can be introduced. This allows the Laplace operator to be represented as $\nabla^2 = \Delta = \left(\frac{\partial^2}{\partial x^2} + \frac{\partial^2}{\partial y^2} + \frac{\partial^2}{\partial z^2}\right) = \left(\mathcal{D}^2 - k^2\right)$.

5.3 System Of Equations

Following the Orr-Sommerfeld and Squire manipulations to the linearised governing equations, the velocity, vorticity and density transport form of the governing equations can be found. The full derivation to reach this result is presented in Appendix A.

$$\left[\left(\frac{\partial}{\partial t}+U\frac{\partial}{\partial x}\right)\nabla^2-\frac{d^2U}{dy^2}\frac{\partial}{\partial x}-\frac{1}{Re}\nabla^4\right]v'+\left[\frac{1}{F_h^2}\left(\nabla^2\cos\theta-\frac{\partial^2}{\partial y^2}\cos\theta+\frac{\partial^2}{\partial y\partial z}\sin\theta\right)\right]b'=0 \tag{5.3.1}$$

$$\left[\frac{\partial}{\partial t}+U\frac{\partial}{\partial x}-\frac{1}{Re}\nabla^2\right]\eta'+\left[\frac{dU}{dy}\frac{\partial}{\partial z}\right]v'+\left[\frac{1}{F_h^2}\frac{\partial}{\partial x}\sin\theta\right]b'=0 \tag{5.3.2}$$

$$\left[\frac{\partial}{\partial t}+U\frac{\partial}{\partial x}-\frac{1}{ReSc}\nabla^2\right]b'-\left[\frac{\cos\theta}{F_h^2}\right]v'+\left[\frac{\sin\theta}{F_h^2}\right]w'=0 \tag{5.3.3}$$

Looking closely at Equation (5.3.1), one can notice that is the stratified form of the Orr-Sommerfeld equation, where the first term is the famous system and the second is the buoyancy contribution. Equation (5.3.2) is the vorticity form of the final system of equations. The first two terms is the famous Squire equation plus the added last term, which is the stratification contribution. Notice that the buoyancy equation (5.3.3) has an unwanted w' term. This can be removed by using the relationship $\tilde{w}=f(\tilde{v},\tilde{\eta})$ which is proved in Appendix A:

$$\tilde{w}=\frac{1}{k^2}\big(i\beta\mathcal{D}\tilde{v}+i\alpha\tilde{\eta}\big) \tag{5.3.4}$$

5.4 Final Equations

Before carrying out the normal-mode solution derivative substitutions, the $\tilde{w}$ term in Equation (5.3.3), which is not one of the reduced state variables, is removed using Equation (5.3.4). Finally substitute in normal mode solution into Equations (5.3.1), (5.3.2) and (5.3.3), while also subbing in Equation (5.3.4) into Equation (5.3.3), to give the three main system of equations:

$$\big[(-i\omega+i\alpha U)(k^2-\mathcal{D}^2)+i\alpha\mathcal{D}^2U+\frac{1}{Re}(k^2-\mathcal{D}^2)^2\big]\tilde{v}+\big[\frac{1}{F_h^2}\big(k^2\cos\theta-i\beta\mathcal{D}\sin\theta\big)\big]\tilde{b}=0 \tag{5.4.1a}$$

$$\big[(-i\omega+i\alpha U)+\frac{1}{Re}(k^2-\mathcal{D}^2)\big]\tilde{\eta}+\big[i\beta\mathcal{D}U\big]\tilde{v}+\big[\frac{1}{F_h^2}i\alpha\sin\theta\big]\tilde{b}=0 \tag{5.4.1b}$$

$$\big[(-i\omega+i\alpha U)+\frac{1}{ReSc}(k^2-\mathcal{D}^2)\big]\tilde{b}+\left[\left(\frac{\sin\theta}{F_h^2k^2}\right)i\beta\mathcal{D}-\left(\frac{\cos\theta}{F_h^2}\right)\right]\tilde{v}+\left[\left(\frac{\sin\theta}{F_h^2k^2}\right)i\alpha\right]\tilde{\eta}=0 \tag{5.4.1c}$$

5.4.1 Matrix System

It would be convenient to put the system of equations into matrix form to give the final eigenvalue problem. Equations (5.4.1a) and (5.4.1c) in matrix form yields:

$$-i\omega\begin{pmatrix}(k^2-\mathcal{D}^2) & 0 & 0\\ 0 & 1 & 0\\ 0 & 0 & 1\end{pmatrix}\begin{pmatrix}\tilde{v}\\ \tilde{\eta}\\ \tilde{b}\end{pmatrix}+\begin{pmatrix}\mathcal{L}_{OS} & 0 & \mathcal{L}_{OS}^b\\ i\beta\mathcal{D}U & \mathcal{L}_{SQ} & \frac{1}{F_h^2}i\alpha\sin\theta\\ \mathcal{L}_v & \big(\frac{\sin\theta}{F_h^2k^2}\big)i\alpha & \mathcal{L}_b\end{pmatrix}\begin{pmatrix}\tilde{v}\\ \tilde{\eta}\\ \tilde{b}\end{pmatrix}=\mathbf{0} \tag{5.4.2}$$

In a more compact form:

$$\mathbf{L}\tilde{\mathbf{q}} = i\omega\mathbf{M}\tilde{\mathbf{q}} \tag{5.4.3}$$

where:

$$\tilde{\mathbf{q}} = \begin{pmatrix} \tilde{v} \\ \tilde{\eta} \\ \tilde{b} \end{pmatrix} \quad \mathbf{L} = \begin{pmatrix} \mathcal{L}_{OS} & 0 & \mathcal{L}^b_{OS} \\ i\beta\mathcal{D}U & \mathcal{L}_{SQ} & \frac{1}{F_h^2} i\alpha \sin\theta \\ \mathcal{L}_v & \left(\frac{\sin\theta}{F_h^2 k^2}\right) i\alpha & \mathcal{L}_b \end{pmatrix} \quad \mathbf{M} = -i\omega \begin{pmatrix} (k^2 - \mathcal{D}^2) & 0 & 0 \\ 0 & 1 & 0 \\ 0 & 0 & 1 \end{pmatrix}$$

$$\mathcal{L}_{OS} = i\alpha U(k^2 - \mathcal{D}^2) + i\alpha\mathcal{D}^2 U + \frac{1}{Re}(k^2 - \mathcal{D}^2)^2 \tag{5.4.4a}$$

$$\mathcal{L}^b_{OS} = \frac{1}{F_h^2}\left(k^2 \cos\theta - i\beta\mathcal{D}\sin\theta\right) \tag{5.4.4b}$$

$$\mathcal{L}_{SQ} = i\alpha U + \frac{1}{Re}(k^2 - \mathcal{D}^2) \tag{5.4.4c}$$

$$\mathcal{L}_v = \left(\frac{\sin\theta}{F_h^2 k^2}\right) i\beta\mathcal{D} - \left(\frac{\cos\theta}{F_h^2}\right) \tag{5.4.4d}$$

$$\mathcal{L}_b = i\alpha U + \frac{1}{ReSc}(k^2 - \mathcal{D}^2) \tag{5.4.4e}$$

Note that terms $\mathcal{L}_{OS}$ is the famous Orr-Sommerfeld coefficient and the buoyancy contribution is represented by $\mathcal{L}^b_{OS}$. Notice that its influence on the Orr-Sommerfeld system reduces with increasing F_h (as stratification strength reduces). $\mathcal{L}_{SQ}$ is the Squire coefficient and its buoyancy contribution is through the term $\frac{1}{F_h^2} i\alpha\sin\theta$. Like the Orr-Sommerfeld system, the stratification influence is reduced with increasing F_h. The matrix system and compact form is following the same nomenclature as page 60 of Schmid and Henningson [10]. The idea was to build on the Orr-Sommerfeld/Squire system solved there. In the limit of $F_h \to \infty$, the matrix system (5.4.2) reduces to the original equations of Schmid and Henningson [10].

5.5 Boundary Conditions

Firstly, looking at the velocity perturbations, $\mathbf{u}'$, the main boundary conditions are imposed from the certain approximations and assumptions that are made. The core assumption of no-slip conditions at the boundaries of the shear plane gives the conditions: $(u', w') = (0, 0)$. Furthermore, exploitation of these conditions along with the fully developed shear velocity profile to the linearised incompressible continuity equation, give the condition: $\mathcal{D}v' = 0$. Next one can employ the non-impenetrable wall assumption. This assumptions implies that the walls at the boundaries of the shear plane will not leak flow, hence velocity perturbations here must be zero, thus this develops the boundary condition: $v' = 0$.

For the pressure perturbation, Dirichlet conditions is normally implemented. As for the buoyancy perturbation, a range of boundary conditions could be used. Lucas [3] imposes the no-flux conditions at the walls, hence has conditions $\mathcal{D}b' = 0$, whereas Facchini [1] sets buoyancy perturbations to zero at the walls. In discussion of their results, Lucas [3] carried out a test case (results were not presented), that suggested applying an insulating wall condition yields very similar results, suggesting a certain robustness in the implemented scheme. For simplicity a Dirichlet buoyancy condition is employed along with the wall-normal voriticity perturbation: $(\eta', b') = (0, 0)$.

So in conclusion, Dirichlet boundary conditions $(v', \eta', b') = \mathbf{0}$ are imposed. The fundamental eigenvalue problem is therefore solved by inputting wavenumbers (α, β) and outputting the eigenvalue $i\omega$.

Chapter 6

Numerical Framework

The fundamental eigenvalue system to be solved is given in Section 5.4.2. This system was to be computed numerically by discretising the equations from a PDE into a matrix operation numerical scheme. The famous scheme that is typically employed is the Chebyshev Transform Method. After that, the solver would be embedded into an algorithm to sort the eigenspectra in order of growth rate with growing stability. Building on top of the algorihm one can generate data like a neutral stability curve and other methods to visualise the eigenspectra and eigenfunctions.

In this Chapter we look to introduce the MATLAB Solver that implements the numerical solver for the system. Discussion of the code's main architecture will be shown first and ways to improve the scripts usability. It was written as a function to optimise its flexibility in many contexts. This requires an overview of the main functions architecture and a discussion of the useful sub-functions that were implemented and before the script could be used to investigate the areas of interest, it must be validated against existing works.

6.1 Numerical Method

As mentioned, the utilised numerical scheme was the Chebyshev Transform Method. It transforms a generic continuous function $u(x)$ into discrete points. More of this will be discussed later but first the stratified solver function architecture must be presented.

6.1.1 `OS_SQ_Stratified_Solver.m`

The main function is named `OS_SQ_Stratified_Solver.m`, which solves the linear stability problem for a stratified Orr-Sommerfeld/Squire system. Generally, the Solver follows the same routine as many scripts with an input, initialisation, solver, post-processing and visualisation. The input parameters are set by the user in the command window. These inputs are firstly validated through a sub-function named `inputValidation.m`. This function ensures that the inputs are of an appropriate data type and value which maximises ease of functionality for the user. Once the inputs are validated, the Solver computes the eigenspectra and outputs three main variables; the domain mesh points in the vertical direction, *ymesh*. This allows the user to plot the perturbed state profiles. The other main outputs include the eigenfunctions of the most unstable eigenmode, *eigenFunction*. This allows the user to produce plots of the perturbation shape of the most unstable growth rate allowing investigation of the stability mechanisms. Finally, the function outputs the ordered eigenspectra, $\omega\_stratSort$, in terms of decreasing instability of the growth rate, ω_i. This is carried out using the sub-function `eigenSort.m`. The remaining secondary functions

include `shearFlow.m`, which determines the velocity profile and its derivatives for the user chosen shear flow and finally the functions `chebdif.m` and `cheb4c.m` determine the Chebyshev derivative matrices, which will be discussed later.

The main inputs to the Solver are $(flow, plotFigure, N, \alpha, \beta, Re, F_h, \theta)$, where $flow$ is the chosen shear base flow (either pCf or pPf), $plotFigure$ is the request for whether the user would like to see plots of the eigenspectra and eigenfunctions, N is the number of Chebyshev grid points, which shall be discussed later, and the rest are the main flow properties that will be studied on their effect to linear stratified stability.

The complete program structure is presented in full in Appendix C. It includes a visualisation of the main steps in performing the LSA of a tilted stratified shear flow (Appendix C.1), displays the outputted command window to the user from running the script (Appendix C.2) and finally all the MATLAB codes are printed (Appendix C.3).

6.1.2 Chebyshev Transform

Now the numerical method that was utilised shall be discussed. The Chebyshev Transform is a type of Discrete Transform Method. They can be viewed as semi-analytical alternatives to finite differences for spatial differentiation applications where high degrees of accuracy are required. These transform methods produce solutions to partial differential equations. A classic type of Discrete Transform Method is the Fourier Series. However, this is not appropriate for representing non-periodic functions as the convergence of the series is rather slow when the number of terms is raised. The Chebyshev polynomial expansion is useful for this application.

An arbitrary smooth function can be represented in terms of a series of orthogonal polynomials, which are the eigenfunctions. An advantage of using polynomial expansions to approximate arbitrary functions is their superior resolution capabilities near boundaries. The arbitrary smooth function, $u(x)$, defined in the domain $-1 \leq x \leq 1$, is approximated by the finite series of Chebyshev polynomials:

$$u(x) = \sum_{n=0}^{N} a_n T_n(x), \tag{6.1.1}$$

where n represents the polynomial order, N is the finite highest order polynomial and a_n represent the Chebshev coefficients with $T_n(x)$ representing the Chebyshev polynomals of order n. The discrete Chebyshev transform representation of u on a discrete set of points is defined as:

$$u_j = \sum_{n=0}^{N} a_n T_n(x_j) = \sum_{n=0}^{N} a_n \cos\frac{n\pi j}{N} \qquad j = 0, 1, 2, ..., N \tag{6.1.2}$$

Note that the smooth functions in this case are the state variables $(\tilde{v}(y), \tilde{\eta}(y), \tilde{b}(y))$ for the domain $-1 \leq y \leq 1$. The function is discretised by the cosine mesh into N points, therefore, $j = 0, 1, 2.., N$. To apply the chosen boundary conditions, j is reduced to $j = 1, 2, ..., N-1$ and profiles for the state variables are found from the eigenfunctions, $(\tilde{v}(y_j), \tilde{\eta}(y_j), \tilde{b}(y_j))$:

$$(\tilde{v}_j, \tilde{\eta}_j, \tilde{b}_j) = \sum_{n=0}^{N} a_n T_n(y_j) = \sum_{n=0}^{N} a_n \cos\frac{n\pi j}{N} \qquad j = 1, 2, ..., N-1 \tag{6.1.3}$$

As well as the state profiles themselves, the state derivative profiles also need to approximated by the Chebyshev polynomials. A more complete understanding of the implemented numerical method can be

found in [11] which is summarised in Appendix B. This method allows the derivatives of the states to be approximated by the Chebyshev matrices found from the secondary functions: `chebdif.m` and `cheb4c.m`.

6.1.3 Chebyshev Grid Point Convergence

In terms of computational cost, it is advantages to minimise the number of Chebyshev grid points used, N. However, using too few grid points would reduce the accuracy of the Chebyshev representation of the smooth function. Therefore, it is useful to carry out a grid point convergence study to evaluate the variation of the solutions as N is increased. The outputted growth rate, ω_i, was examined and plotted against N for both shear flows; pCf and pPf. The analysis allowed us to determine the required number of grid points until the results convergence, in other works, the results do not change from a further increase in N.

The convergence plot can be observed in Figure 6.1, where the two curves represents the study carried out for the pCf and pPf. For the convergence study, Re and F_h were held constant at values of 1000 and 1, as their value has no significance on convergence. θ was arbitrarily set to 30 degrees and $(\alpha, \beta) = (1, 1)$.

For completeness, the convergence of N should be determined for a range of input parameters to prove its independence on the accuracy of the solution. The other simulations that were run for different values of θ and (α, β) are shown in Appendix C.4. One should observe how the input parameters have no influence on the convergence of the solution as all the curves appear to converge at the similar points. All the curves illustrate the same features, they convergence at $N \approx 100$ and then begin to diverge once again at $N \geq 200$. The latter suggests the existence of Gibbs phenomenon where the solution typically divergences at large mesh densities, which is a particularly common result as described in [12]. Therefore, an appropriate value for N would be within the range: $100 \leq N \leq 200$. To minimise computation cost and reinforced by other works, the number of grid points for all simulations was at a value of: $N = 100$.

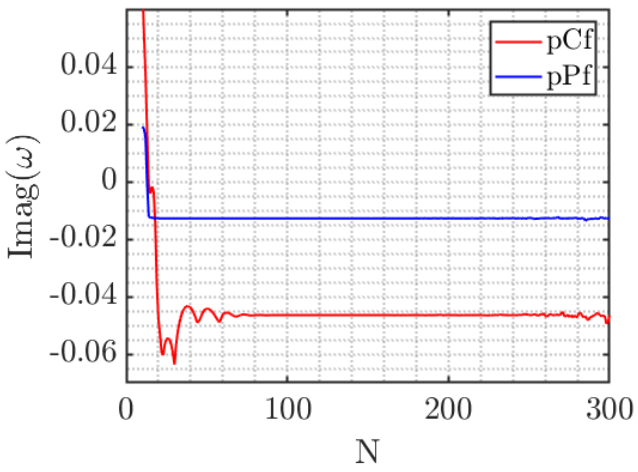

Figure 6.1: Convergence of the growth rate with varying the Chebyshev grid points for both the pCf and pPf.

6.2 Implementing Boundary Conditions

As discussed, Dirichlet boundary conditions for each state variable were implemented: $(\tilde{v}, \tilde{\eta}, \tilde{b}) = \mathbf{0}$. These conditions could be intuitively imposed by removing the outer bracket of the resulting Chebyshev matrices by removing the first and last rows and columns. This would create spurious modes, hence a more elegant method was proposed by embedding the clamped condition right within the fourth order Chebyshev differential matrices. Weideman and Reddy [13] provides the MATLAB function `cheb4c.m` which generates the fourth order Chebyshev differential matrices with the clamped conditions embed, while `chebdif.m` generates the Chebyshev differential matrices of the first three orders.

6.3 Validation Approach

The solver was designed to maximise re-usability and flexibility for further work thus it was important to ensure the script could be built on for other systems and base flows. To achieve this, the solver must firstly be validated against existing research. Data was used from multiple sources; mainly Schmid and Henningson [10] and Facchini [1]. It is important that as many aspects of the script was validated. It is important to notice that there are slight discrepancies between the approaches taken to reach the final eigenvalue problem. For example, Facchini [1] does not use the Orr-Sommerfeld governing equations. Adding shear flows to the solver is simply done through adding the velocity profiles in the `shearFlow.m` function, while ensuring the new base flow has a tag when called by the shear flow input, *flow*.

6.3.1 Unstratified Case

The solver was firstly developed from a Orr-Sommerfeld/Squire system with an unstratified pCf and pPf flow. This allowed direct validation with the Schmid and Henningson [10], which contains data of the most unstable eigenmodes of the pCf and pPf under defined conditions.

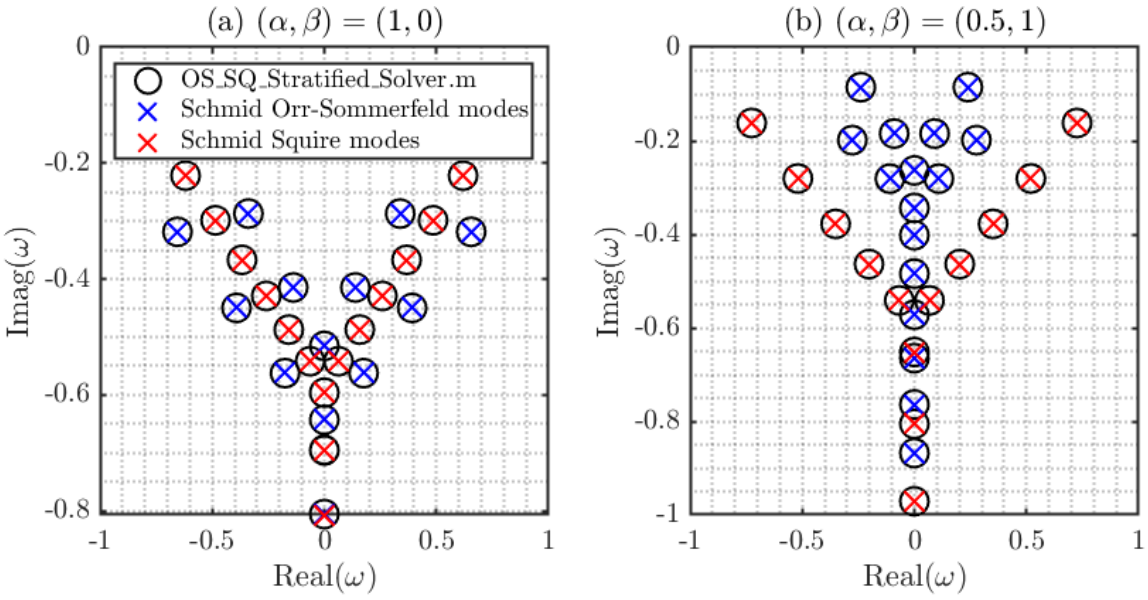

Figure 6.2: Comparison of the eigenspectra on the ω complex plane for different wavenumbers with the pCf.

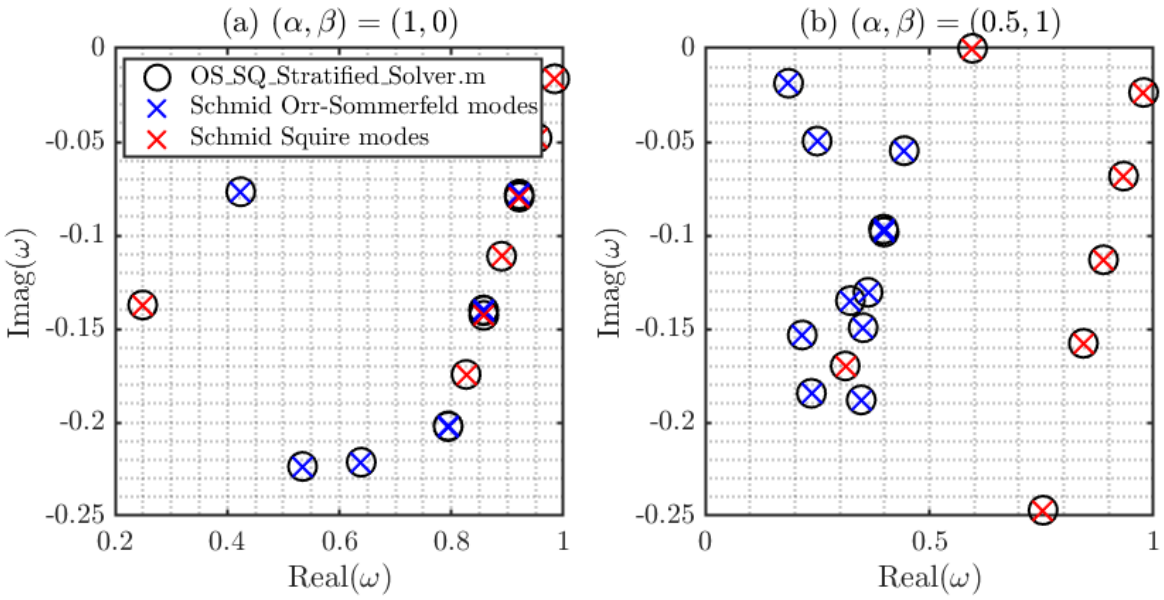

Figure 6.3: Comparison of the eigenspectra on the ω complex plane for different wavenumbers with the pPf.

Figure 6.2 shows the data points of the eigenspectra from state variables $(\tilde{v}, \tilde{\eta})$ for the pCf. The inputs were Re of 800 and the wavenumbers, (α, β), were $(1, 0)$ and $(0.5, 1)$ for Figures 6.2(a) and (b) respectively. One can note how the eigenvalues match exactly with the Schmid Orr-Somerfeld and Squire modes. Similarly, Figure 6.3 shows the eigenspectra for the pPf, with a Re of 2000 but with the same wavenumbers as the pCf case. Again the eigenvalues from my unstratified solver matched Schmid's results exactly.

Further validation was carried out for the unstratified case using the pPf. A famous result is that the transition Re for $(\alpha, \beta) = (1, 0)$ is 5772 (refer to [8]) which the solver outputs. Likewise, for input parameters $(\alpha, \beta, Re) = (1, 0, 10000)$, the most unstable eigenmode has value $0.2375 + 0.0037i$, a key result presented in [8]. These results proved that the developed unstratified solver was working as expected and now the stratification was simply needed to be implemented. To the end, the state varable $\tilde{b}$ needed to be added to the system. The new system needed to converge to the unstratified case as $F_h \to \infty$, as this represents a negligible stratification strength.

6.3.2 Stratified Case

Facchini [1] carried out LSA on a pCf with spanwise stratification. One of Facchini's main results was that one stationary growing mode appears at $(\alpha, \beta, Re, F_h) \approx (0.8, 5, 1000, 1)$. This produced ω with $\omega_r = 0$ and $\omega_i > 0$. Inputting these variables into the solver `OS_SQ_Stratified_Solver.m`, with tilt angle at 90 degrees, outputted a single unstable mode with value: 0.0000 + 0.0127i. This matches the findings of Facchini exactly.

Following this result, Facchini produces a plot of the full eigenspectra of the most unstable mode at $Re = 1000$ and $F_h = 1$, with wavenumbers $(0.815, 4.937)$. The plot is shown in Figure 6.4(b), while the result produced from the developed solver is shown in Figure 6.4(a).

The significant result is the single unstable eigenmode that crosses the ω_i axis. Figure 6.4 magnifies this result through the inset which is the area delimited by the red triangle, expressing the single unstable mode.

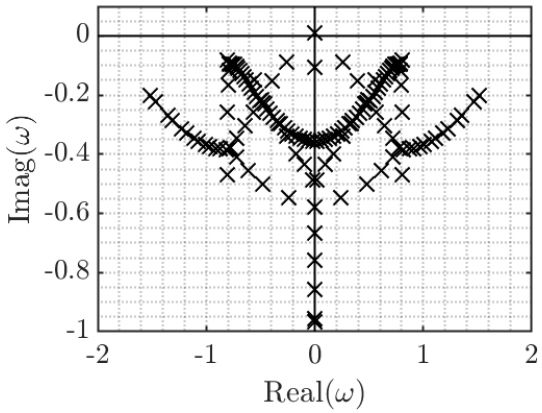

(a) Result from `OS_SQ_Stratified_Solver.m`.

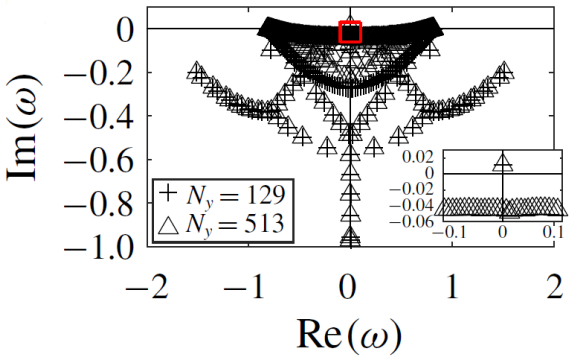

(b) Result from Facchini [1].

Figure 6.4: Complex plane plot of ω with input parameters $(\alpha, \beta, Re, F_h) = (0.815, 4.937, 1000, 1)$. (b) Note that $Re(\omega)$ represents the oscillatory frequency and $Im(\omega)$ is the growth rate.

The result from the solver matches this result as a lone eigenvalue exists in the upper half plane. Likewise, notice how the shape of the eigenspectra is similar providing further support for the accuracy of the developed solver. There are some differences however which would be important to note. Facchini's result has a much richer eigenspectra given that the state variables implemented were $(\tilde{\mathbf{u}}, \tilde{p}, \tilde{b})$. This reinforces the decision to reduce the state variables to mitigate the computational cost. Moreover, Figure 6.4 plots $N = 129$ and 513, whereas the solver uses $N = 100$. Notice how Facchini's result does not appear to exhibit Gibb's phenomenon at $N > 200$ suggesting that the numerical system used is well resolved, however at the expensive of a large computational cost.

Finally, we will validate the outputted eigenfunctions from the solver. Figures C.6 and C.7, in Appendix C.5, show the velocity and buoyancy perturbations with input parameters $(\alpha, \beta, Re, F_h) = (0.767, 4.937, 10000, 1)$ with results obtained from the solver and Facchini.

Note that the wall-normal voriticity perturbation could not be validated as it was not a state variable used by Facchini. Observing each Figure we can see that the shapes of the perturbations matches exactly. There are some discrepancies, which appears from the differences in the systems employed. Also, Facchini normalises the perturbations with the maximum perturbation in the u-field, whereas the solver does not normalise the eigenfunctions.

As a final result, it is useful to check whether the stratified system converges to the original Orr-Sommerfeld/Squire system in the limit of $(Re, Sc) \to \infty$, which is does. This can be easily observed by looking at the system of Equations (5.4.2), where it is clear to observe that all the buoyancy contributions, $\tilde{b} \to 0$ in this limit as the contributions are inversely proportional to F_h.

Chapter 7

Results and Discussion

This chapter will review the main results that were generated from the developed MATLAB Solver; `OS_SQ_Stratified_Solver.m`. The results were found from varying the main inputs, while fixing the Schmid number at 700. Likewise, from the convergence study discussed in the previous section, the number of Chebyshev grid points was fixed to a value of 100. The remaining input parameters that were varied are $(\alpha, \beta, Re, F_h, \theta)$ for a chosen base profile; either pCf or pPf. With these parameters, the most unstable eigenmode was extracted, $\omega_{i,max}$. Likewise, the eigenfunctions of the most unstable eigenmode could be outputted should the user request it.

Given time, a broad range of tilt angles could have been studied to fully investigate the inalignment influences. However, due to time restricts, the main angles that were investigated were 5, 30, 60, 80 degrees, where 5 and 80 degrees were to represent a small and heavy tilt angle. This would give us a strong indication of how the behaviour of the flow evolves from the aligned stratification case to the spanwise case.

The results were categorised into varying certain input parameters while holding the remaining parameters constant. Firstly, the outputted eigenspectra was examined to provide an insight on the features of the complex frequency. Next, the wavenumbers were swept to find the region where instabilities are found. As stated by Deloncle [7], two-dimensional instabilities are not expected to dominate, hence reinforcing an interest in three-dimensional turbulence thus non-zero values of (α, β). Next the influence of the tilt angle on the critical Reynolds number, Re_{crit} shall be analysed. Furthering our interest in Re, investigation on the influence of Re on the growth rate is carried out. After that, the F_h effects are examined and finally investigation of the eigenfunctions allow the visualisation of the perturbations providing an idea on the stability mechanisms. Finally, brief comments on the influence of Sc shall be included.

More analysis on the pCf will be presented in the following Sections, particularly in the cases when the pPf results follow similar trends to the pCf. The Figures for the pPf in these cases with be in Appendix D.

7.1 Eigenspectra

Below plots of the eigenspectra for the pCf and pPf are presented in Figures 7.1 and 7.2 respectively. The input parameters where $(Re, F_h) = (10000, 1)$ for both base flows and the wavenumbers were $(\alpha, \beta) = (0.8, 5)$ for the pCf and $(\alpha, \beta) = (1.5, 6)$ for the pPf. These wavenumbers were chosen as these are the primary regions of instability that appears as the tilt angle increases. This will be made clearer in the neutral stability plots to be presented in Section 7.2. The tilt angle was varied and the subplots in the Figures show the results for $\theta = 5$, 30, 60 and 80 degrees. Both Figures have red points which represents the most unstable eigenmode.

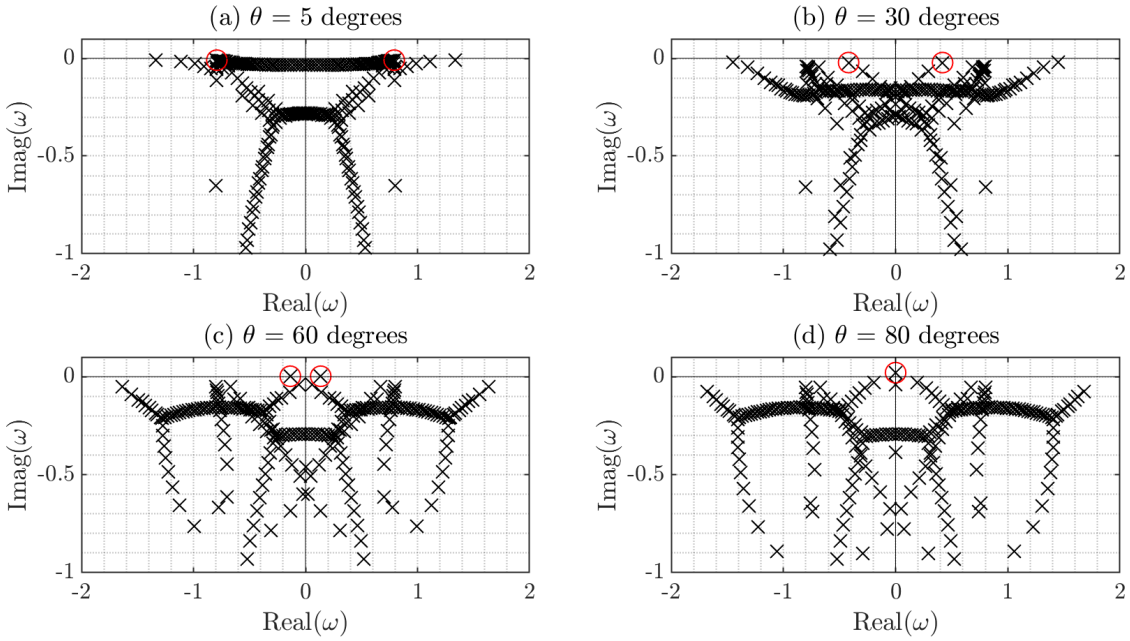

Figure 7.1: Eigenspectra of the pCf base fluid with inputs $(\alpha, \beta, Re, F_h) = (0.8, 5, 10000, 1)$ with subplots of varying tilt angle θ.

Observing Figure 7.1, one can notice how the eigenspectra has a symmetrical feature with respect to the real axis, where for a certain growth rate, there is a conjugate pair. One can observe how the eigenmodes break down into various branches as the inalignment is strengthened. This illustrates how the shear and stratification tilt produces more complex flow structures. However, the most significant eigenmode is with most unstable growth rate (highlighted in red). The value of ω_i becomes more positive as the tilt angle is raised. This suggests that the inalignment has a destabilising consequence to the base flow. Notice how as the tilt angle increases, the oscillatory frequency of the most unstable mode (ω_r) decreases in magnitude, as the conjugate pairs move closer together. Between the inalignment angle; 60 degrees and 80 degrees, the most unstable eigenmodes coalesce to produce a single unstable eigenmode with zero oscillatory frequency. Facchini (2018) found the same result, that at 90 degrees, for the critical (Re, F_h), the single unstable mode was non-oscillatory. It is key to note that the instability does not arise at the moment of coalescence, as through observing Figure 7.1(c), the two conjugate eigenmodes are in the upper half plane.

Now looking at Figure 7.2, the symmetry of the eigenvalues does not appear. The eigenspectra is dominated in the lower right plane, with an array of eigenmodes with positive ω_r and stable ω_i. Like the pCf, the most unstable eigenmode becomes more unstable as the tilt angle increases, so the stratification shear inalignment continues to destablise the pPf base flow as well. Moreover, as the tilt angle increases, the eigenspectra splits into multiple branches which also shows the increase in complexity of the perturbations as the tilt angle increases. This displays signs of consistency of the influence of stratification inalignment to the stabililty of shear flows. However, unlike the pCf, there only exists a single unstable mode at all tilt angles. Note that the symmetrical and assymmetrical features of the eigenspectra, for the pCf and pPf respectively, is also found in the unstratified case with the Orr-Sommerfeld and Squire system, shown in Figures 6.2 and 6.3.

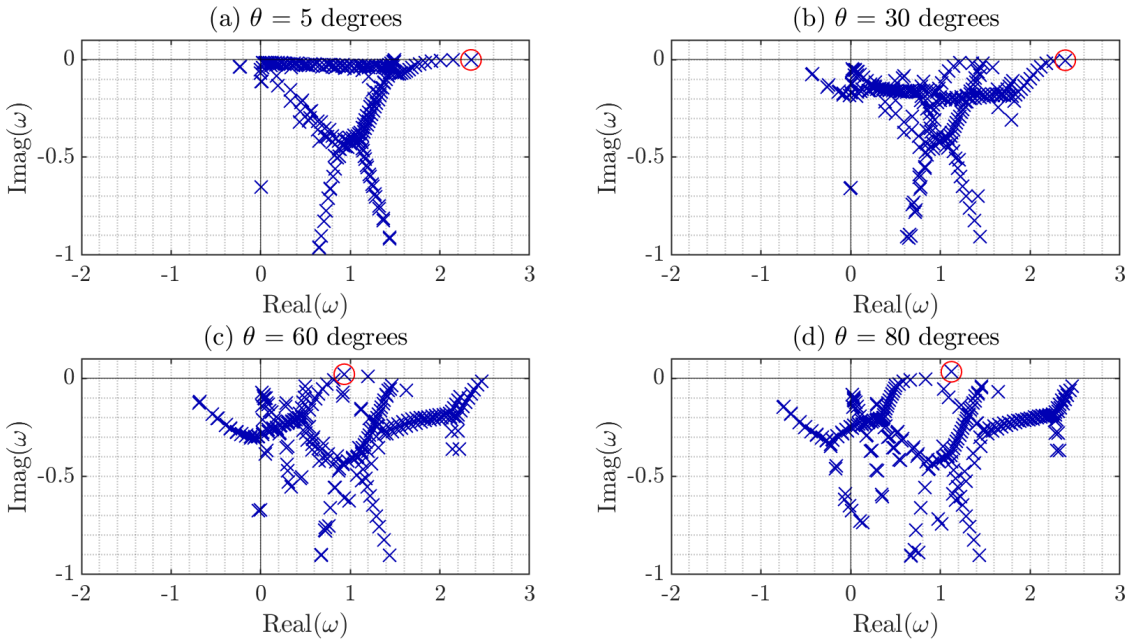

Figure 7.2: Eigenspectra of the pPf base fluid with inputs $(\alpha, \beta, Re, F_h) = (1.5, 6, 10000, 1)$ with subplots of varying tilt angle θ.

7.2 Sweeping Wavenumbers, (α, β)

As a first result, it would be useful to find the region of instability in the wavenumber state space. Therefore, this requires neutral stability plots which are shown in Figures 7.3 to 7.6.

To this end, the stratified solver was run sequentially for a range of wavenumbers while fixing parameters $(Re, F_h, \theta) = (10000, [1, 0.5], [5, 30, 60, 80])$. Figures 7.3 and 7.4 are for the pCf and Figures 7.5 and 7.6 are for the pPf. In these Figures, subplot (a) represents a tilt angle of 60 degrees and (b) with a tilt angle of 80 degrees. Note that results for an inalignment of 5 and 30 degrees has not been shown, as the flow was found to always be stable in these cases. This result is consistent with what was found in the eigenspectra plots of Section 7.1. Notice each of the plots exhibit a red cross. This point represents the most unstable eigenmodes. It is interesting to note that this point is the same for each base flow, which suggests the most unstable point is independent of F_h and θ.

Observing Figure 7.3, the instability bubble is found around the range of wavenumbers $(\alpha, \beta) = ([0.7, 0.8], [4, 5])$. As the tilt angle increases, the instability bubble appears around this region and exhibits slow growth, in the wavenumber plane, which continues until the stratification is aligned spanwise. The area of this instability region is relatively small compared with the pPf cases suggesting that stratified pCf instability is uncommon.

Next, looking at the influence of F_h, by comparing Figures 7.3 and 7.4, increasing the stratification appears to destabilise the flow for a certain tilt angle as the instability region is of a higher area. The increase in the range of instability is small in α, however for β the flow destabilises for almost seven times the range when F_h was decreased from 1 to 0.5. To give us a deeper understanding of this finding, further analysis on the influence of F_h to the stability of tilted stratified shear will be included in Section 7.4.

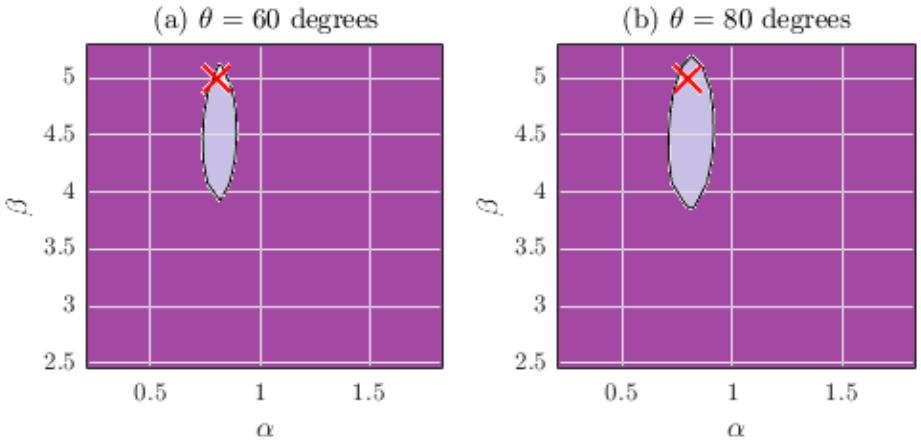

Figure 7.3: Neutral stability plots in the wavenumber state space for the pCf. The instability region is shown in light purple, with the dark purple region being the stable area. The red cross marks the most unstable point. The input parameters were $(Re, F_h) = (10000, 1)$ and (a) $\theta = 60$ degrees, (b) $\theta = 80$ degrees.

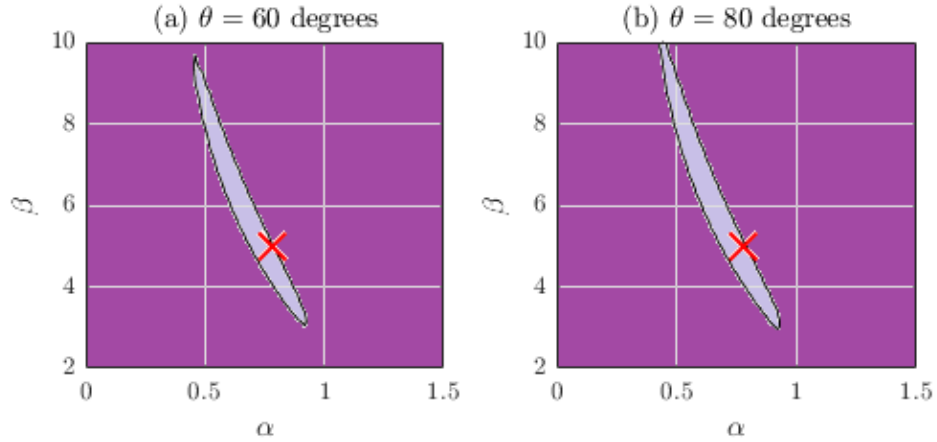

Figure 7.4: Neutral stability plots in the wavenumber state space for the pCf. The instability region is shown in light purple, with the dark purple region being the stable area. The red cross marks the most unstable point. The input parameters were $(Re, F_h) = (10000, 0.5)$ and (a) $\theta = 60$ degrees, (b) $\theta = 80$ degrees.

Now observing Figures 7.5 and 7.6 which were results for the pPf, there is a noticeably larger region of instability in the wavenumber state space with respect to the pCf. This is a particularly expected result as the unstratified pPf is more unstable than the pCf. Once again, by increasing the stratification (by reducing F_h), the region of instability grows, as found with the pCf. This can be seen as the unstable bubble is much larger for the respectively tilt angle between the two Figures. Likewise, as the tilt angle increases, the instability bubble grows. However, unlike the pCf, the most unstable region (marked with the red cross), is found around the centre of the instability region. This could suggests that at the critical tilt angle, the instability region is likely to be introduced at this point and then propagate in the wavenumber space as tilt angle is raised. The most unstable region for the pCf was at the point $(\alpha, \beta) = (0.8, 5)$ (as found by Facchini [1]) and $(1.5, 6)$ for the pPf.

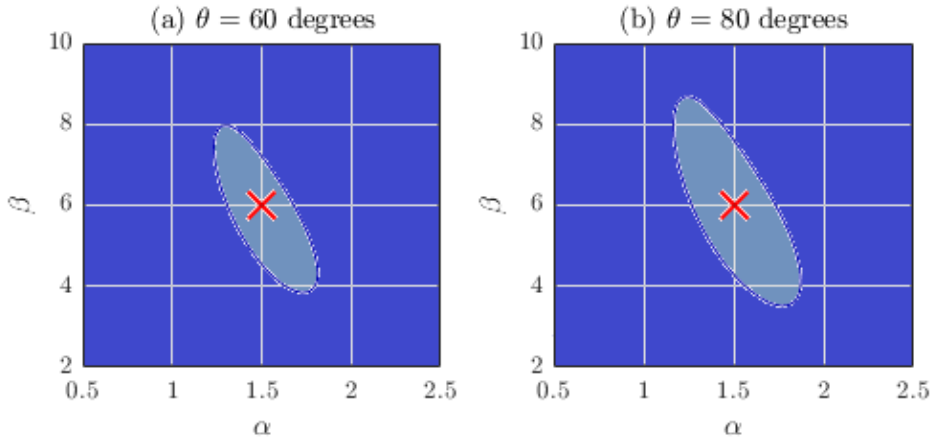

Figure 7.5: Neutral stability plots in the wavenumber state space for the pPf. The instability region is shown in light blue, with the dark blue region being the stable area. The red cross marks the most unstable point. The input parameters were $(Re, F_h) = (10000, 1)$ and (a) $\theta = 60$ degrees, (b) $\theta = 80$ degrees.

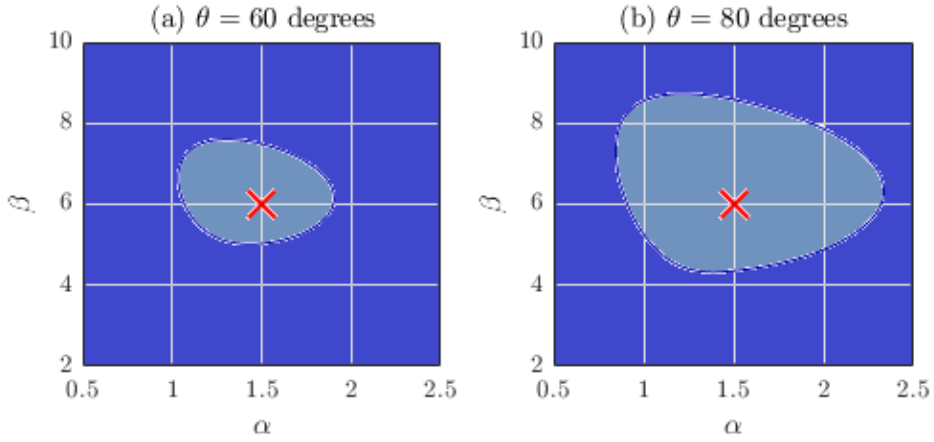

Figure 7.6: Neutral stability plots in the wavenumber state space for the pPf. The instability region is shown in light blue, with the dark blue region being the stable area. The red cross marks the most unstable point. The input parameters were $(Re, F_h) = (10000, 0.5)$ and (a) $\theta = 60$ degrees, (b) $\theta = 80$ degrees.

7.3 Effect Of Reynolds Number, Re

Next, examination of the influence of Re on the linear stability of the stratified shear flow shall be carried out. Firstly, it is useful to plot the transitional Reynolds number, Re_{crit}, against the tilt angle which is presented in Figure 7.7. This includes results for both shear flows; (a) pCf and (b) pPf. The input parameters were held at constant values equal to (a) $(\alpha, \beta, F_h) = (0.8, 5, [0.95, 1, 1.05])$ and (b) $(\alpha, \beta, F_h) = (1.5, 6, [0.95, 1, 1.05])$. Notice that the chosen wavenumbers for each shear profile were based on the most unstable point found in the neutral stability plots in Section 7.2. Each curve represents cases with a different F_h. Both plots exhibit the trend that as F_h is reduced, the curves shift to the left which illustrates a loss in stability, as for a certain tilt angle, the transitional Re decreases in value. This provides more evidence in how increasing the stratification strength results in a destabilising effect.
Furthering the analysis on the influence of the F_h to Re_{crit}, the lines of best fit have an exponential profile. This allows an empirical approximate for the transitional point of Re for a given θ and F_h. From examining the three F_h results, for the pCf case, the critical Reynolds number can be reasonably approximated as a

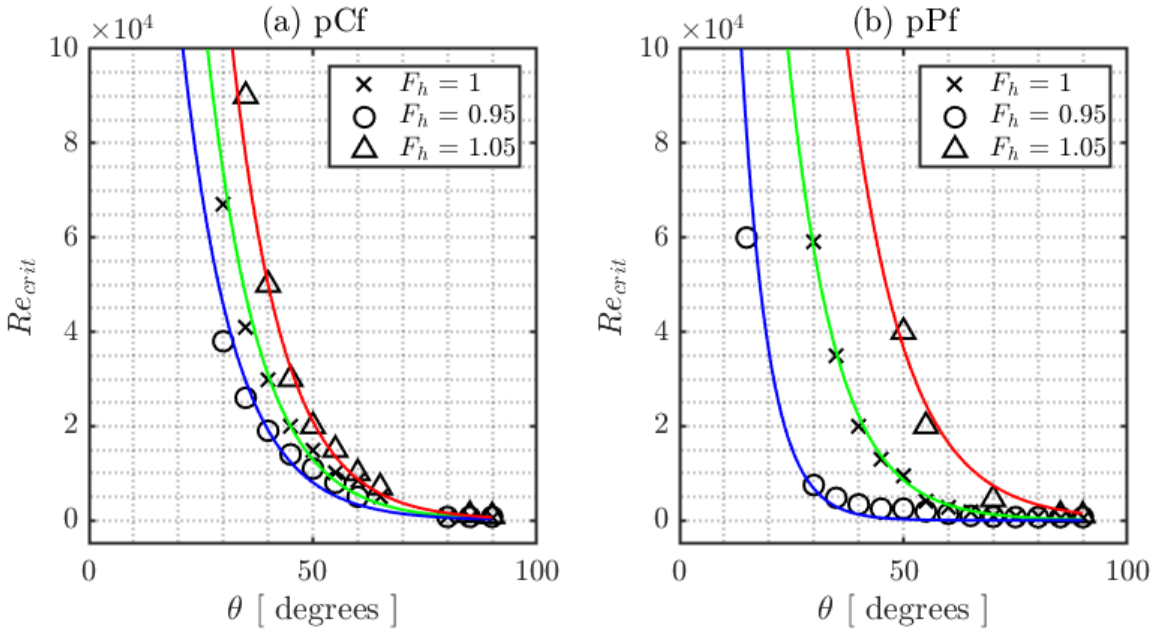

Figure 7.7: The transitional Re for different inalignment angles, with various curves for $Fh = 0.95, 1, 1.05$. A line of best fit is applied to each data set to provide a relationship between the tilt and the critical Re. The red curve represents the case with $F_h = 1.05$, blue curve is for the case with $F_h = 0.95$ and the green curve is for $F_h = 1$.

function of the tilt and Froude number, $Re_{crit} = f(F_h, \theta)$, presented below:

$$Re_{crit}(F_h, \theta) = \big((4.8 \times 10^7)F_h^2 - (8.6 \times 10^7)F_h + (3.9 \times 10^7)\big)\exp\big(-0.087\theta\big) \tag{7.3.1}$$

It can be seen that $Re_{crit} = f_1(F_h)\exp(f_2(\theta))$, where $f_1(F_h)$ is a quadratic function in terms of Froude number and $f_2(\theta)$ is a linear function in terms of tilt angle. As for the pPf, the relationship $Re_{crit} = g(F_h, \theta)$ is slightly more complicated:

$$Re_{crit}(F_h, \theta) = \big((2 \times 10^8)F_h^2 - (3.9 \times 10^8)F_h + (1.9 \times 10^8)\big)\exp\left(\frac{\theta}{-500F_h^2 + 1065F_h - 554.5}\right) \tag{7.3.2}$$

in which $Re_{crit} = g_1(F_h)\exp(g_2(F_h, \theta))$ where $g_1(F_h)$ is a quadratic function in terms of Froude number and $g_2(F_h, \theta$ is function of both F_h and θ. Note that Equation (7.3.1) can only be applied in the range $20 \leq \theta \leq 90$ degrees, below 20 degrees one can assume the flow to always be stable. As for Equation (7.3.2), it is only valid for tilt range $10 \leq \theta \leq 90$ degrees, again below 10 degrees the flow is always stable. Moreover, the Equations (7.3.1) and (7.3.2) can only be applied for a suitable F_h range ($0.95 \leq F_h \leq 1.05$) and must be reiterated that they are empirical approximations. Both the pCf and pPf have an exponential decay in the transitional Reynolds number as the inalignment is increased towards spanwise stratification. This suggests the influence of the tilt has a significant effect at moderate angles, where there is a significant destabilisation between angles 30 to 50 degrees for the pCf. The F_h has more of an influence on where a significant drop in stability occurs.

Moreover, in development of understanding the influence of Re on stability, a plot of the growth rate of the most unstable mode changes with Re, presented in Figure 7.8. This is for the pCf case only. The input parameters in this case were $(\alpha, \beta, F_h, \theta) = (0.8, 5, 0.4, [5, 30, 60, 80])$, where the subplots represent different

unalignment angles. Observations of rapid saturation to a constant value is apparent, as Facchini [1] also found. The converged solution in every case is to the inviscid solution. Thus, one can conclude that the instabilities must reply on inviscid mechanisms and it is fair to use an inviscid approximation to capture the spatial and temporal features of the most unstable mode. The results for the pPf is not presented here, but featured in Appendix D, where the pPf exhibits similar results.

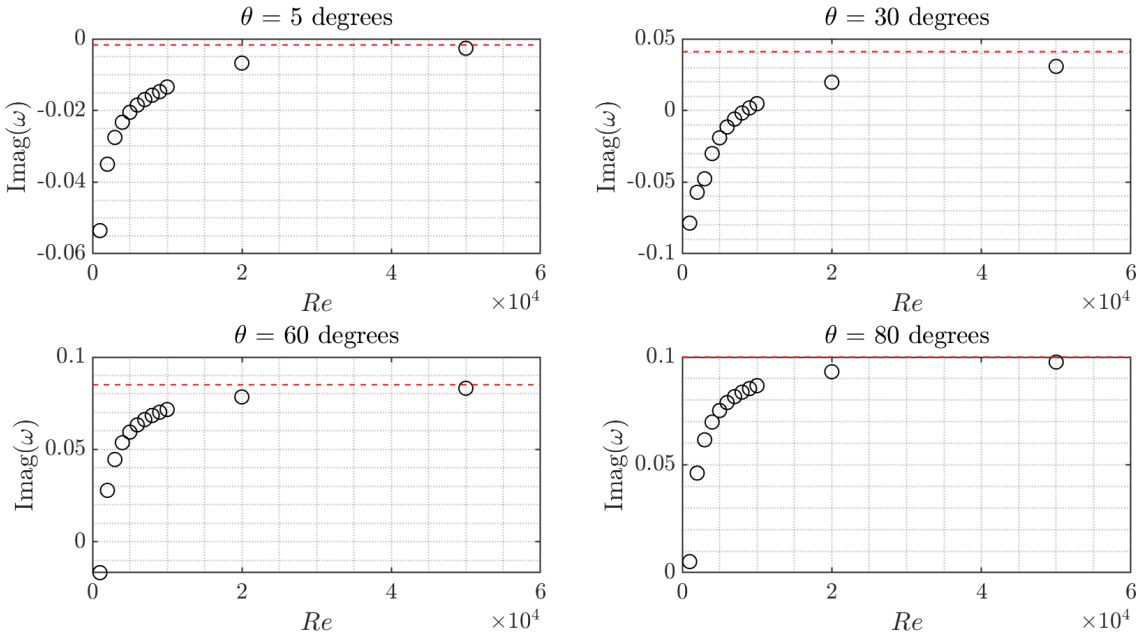

Figure 7.8: Growth rate, ω_i, of the most unstable mode as a function of Re with $(\alpha, \beta, F_h) = (0.8, 5, 0.4)$ and θ = (a) 5, (b) 30, (c) 60 and (d) 80 degrees.The red dotted line represents the inviscid solution in the limit $Re \to \infty$.

7.4 Effect Of Stratification, F_h

An interesting feature of the previous results was the apparent destabilisation caused by reducing F_h, which is a fairly counter-intuitive result as the stratification is found to suppress turbulent growth in the aligned case. To study the influence of the stratification strength, analysis of the growth rate as a function of F_h is presented in Figures 7.9 and 7.10, which represents the pCf and pPf respectively. Re was held constant at 1000 in both cases, the most unstable wavenumbers for each shear was implemented and the tilt angle was varied to produce the subplots. Observing both Figures, there is a clear trend where as the stratification is strengthened, from a weakly stratified case ($F_h > 1$), the increased stratification strength stabilises the flow, as the growth rate becomes more negative when the F_h is decreased from 1.5.

However, interestingly, a further decrease in the F_h illustrates a destabilising feature as decreasing F_h increases the growth rate. The point at which the stratification starts to destabilise the shear can be defined as the critical Froude number, $F_{h,crit}$. Then at extreme stratification strengths, generally around $F_h < 0.4$, the flow re-stabilises with increasing stratification; this point can be defined as the restabilising F_h. Figure 7.10 shows this trend much clearer. One can observe how as the unalignment angle is raised, $F_{h,crit}$ moves further right in the F_h plane, along with the re-stabilisation F_h. For clarity this is tabulated

in Table 7.1. By closely evaluating the values, one can observe the range of F_h which destabilises the pPf for the given tilt.

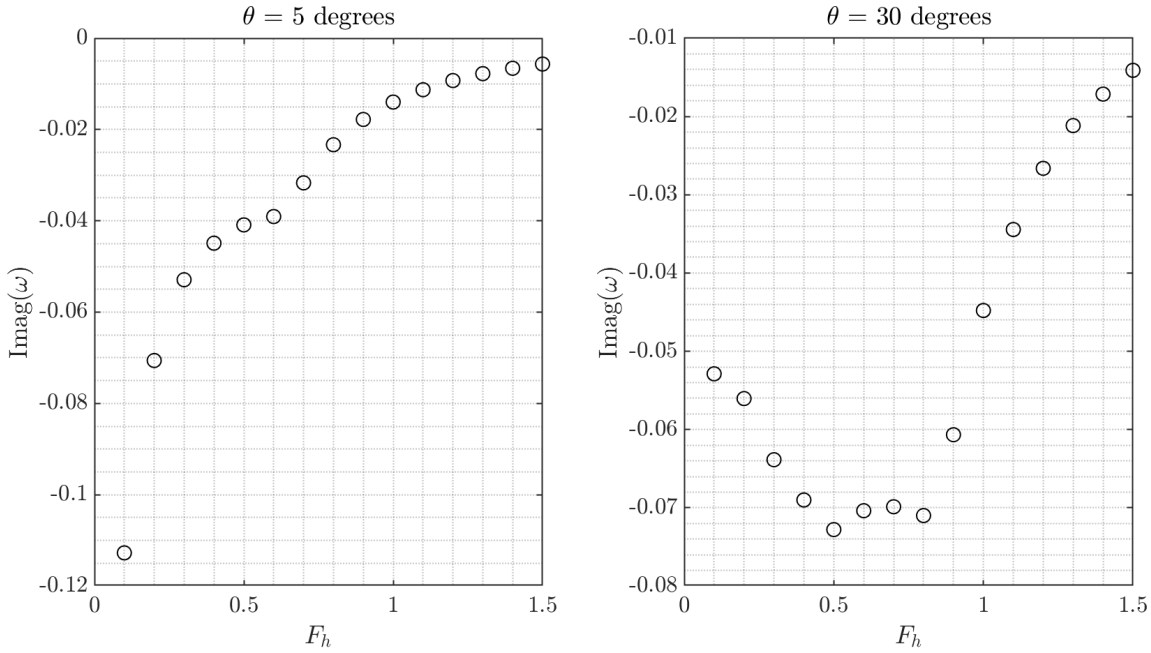

Figure 7.9: Growth rate against F_h for the pCf with input parameters $(\alpha, \beta, Re) = (0.8, 5, 1000)$ and $\theta =$ (a) 5, (b) 30 degrees.

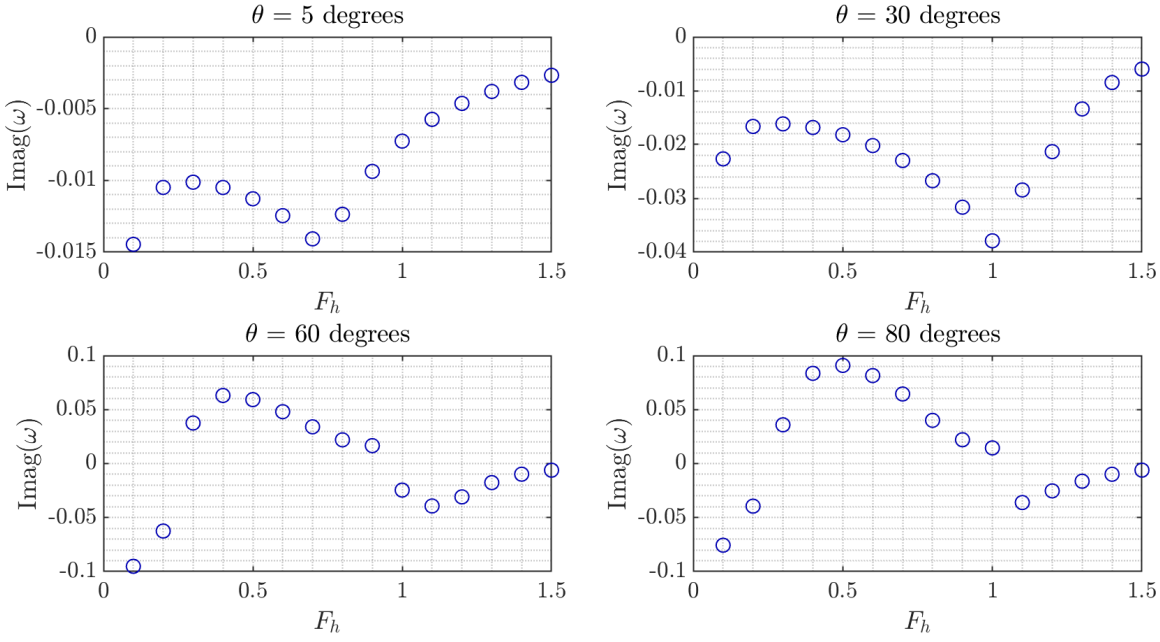

Figure 7.10: Growth rate against F_h for the pPf with input parameters $(\alpha, \beta, Re) = (1.5, 6, 1000)$ and $\theta =$ (a) 5, (b) 30 degrees, (c) 60 and (d) 80 degrees.

Table 7.1: Critical F_h and re-stabilisation F_h for a given inalignment angle in a pPf shear. The destablisation zone can be defined as the range over which decreasing F_h destabilises the shear flow.

θ [deg]	$F_{h,crit}$	Re-Stabilisating F_h	Destabilisation Zone
5	0.7	0.3	0.4
30	1	0.3	0.7
60	1.1	0.4	0.7
80	1.1	0.5	0.6

It appears that $F_{h,crit}$ increases with the tilt angle but converges to 1.1 around an unalignment angle of 60 degrees. Likewise, the destabilisation zone grows with the tilt, therefore there is a greater region of destabilising effects for higher unalignment angles. Like the critical Froude number, its value also seems to converge. There seems to be a small difference between the restabilisation point. Looking back at Figure 7.10, the magnitude of the destabilisation effect grows with a higher tilt angle. This is apparent as the gradient of which the growth rate rises in the destabilisation zone for each tilt angle increases with θ.

7.5 Effect Of Unalignment, θ

Investigation of the unalignment angle on the shear flow stability was carried out next. Figure 7.11 was produced by evaluating the growth rate at different tilt angles for the pCf. The input parameters were held constant as $(\alpha, \beta, Re, F_h) = ([1, 0.8], [0, 5], 1000, 1)$. Figure 7.11(a) represents the 2D case where $\beta = 0$, and one can observe how the tilt has a stabilising effect. This reinforces the theory that 2D instabilities do not dominate in this scenario.

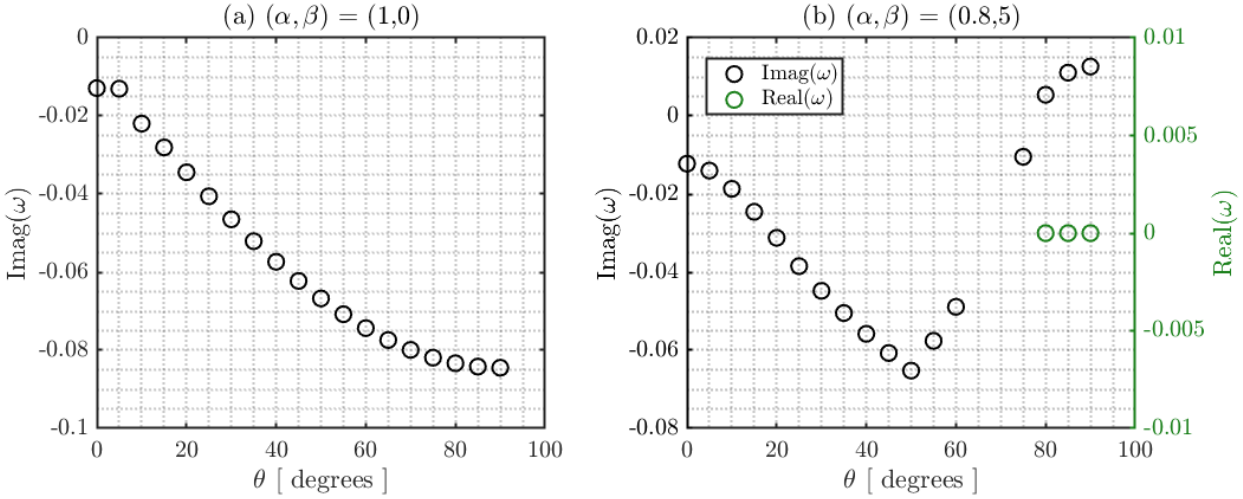

Figure 7.11: Growth rate against the tilt angle for inputs $(Re, F_h) = (10000, 1)$ and (α, β) = (a) (1, 0) and (b) (0.8, 5). (b) The oscillatory frequency, ω_r, is plotted for the unstable modes found at the high tilt angles. These values are plotted in green and are with respect to the right green axis.

Now observing Figure 7.11(b), the tilt angle is surprising stabilising between angles 0 degrees to 50 degrees, where as the inalignment is raised this stabilises the flow. This is an interesting feature, however it mainly just shows how the flow still remains stable for small tilt angles. Then, as the tilt angle is raised beyond 50 degrees the flow destabilises as the growth rate becomes more positive. An angle of 80 degrees induces

instabilities and the flow then becomes unstable from this point. The oscillatory frequency of the unstable modes are plotted alongside the growth rate. It is interesting to note how ω_r remains non-oscillatory displaying the nature of the perturbation growth. This is consistent with the coalescence that was found in the eigenspectra in Section 7.1.

Results for the pPf are presented in Appendix D as they produce findings similar to the pCf case. However, by comparing Figures 7.11(b) and D.2(b) (in Appendix D), the oscillatory frequency for the unstable modes are non-zero in the pPf case but purely non-oscillatory in the pCf case.

7.6 Eigenfunction

So far the main focus has been on the features of the unstable eigenmodes and under which conditions they appear, given the combination of the parameters $(\alpha, \beta, Re, F_h, \theta)$. These values allow characterisation of the instability but provides no information on the mechanisms that cause them. To achieve an understanding on this requires visualisation of the shapes of perturbations for the unstable modes. The idea that the instability relies on an inviscid mechanism has already been realised, however, as Facchini [1] explains, implementing the inviscid eigenvalue problem induces spurious unstable modes making detection of genuine instability difficult. Hence, it is useful to keep the Re finite but reasonably large to ensure capture of all the instability features, thus Re was held constant at 80000. To report the shapes of the perturbations requires analysis of the eigenfunctions, which is displayed in Figures 7.12 to 7.14 below. These Figures are the perturbed shapes of each of the state variables (a) $\tilde{v}(y)$, (b) $\tilde{\eta}(y)$ and (c) $\tilde{b}(y)$, where Figure 7.12, 7.13 and 7.14 represent the eigenfunctions for a tilt angle of 5, 60 and 80 degrees respectively.

Analysing each Figure separately, 7.12 shows weak and near negligible perturbations in the upper half plane of the shear plane, where the perturbations are dominant in the lower half plane for all the state variables. As the tilt angle is increased to 60 degrees, Figure 7.13, shows how the perturbations then propagate to the upper half plane, but still remain larger in the lower half plane. The vertical velocity perturbation and buoyancy perturbation are more important closer to the wall boundaries ($y = \pm 1$), and the perturbations drop close to zero in the middle of the shear plane. On the contrary, the wall-normal vorticity profile has a near-constant gradient drop in the pertubation from the lower wall to the upper wall. Finally, at an inalignment angle of 80 degrees, Figure 7.14 shows quasi-symmetrical perturbation profiles as the stratification tends to a spanwise direction. For high tilt angles, all the state variables have perturbations that dominate closer to the walls and are negligible at the centre of the shear plane.

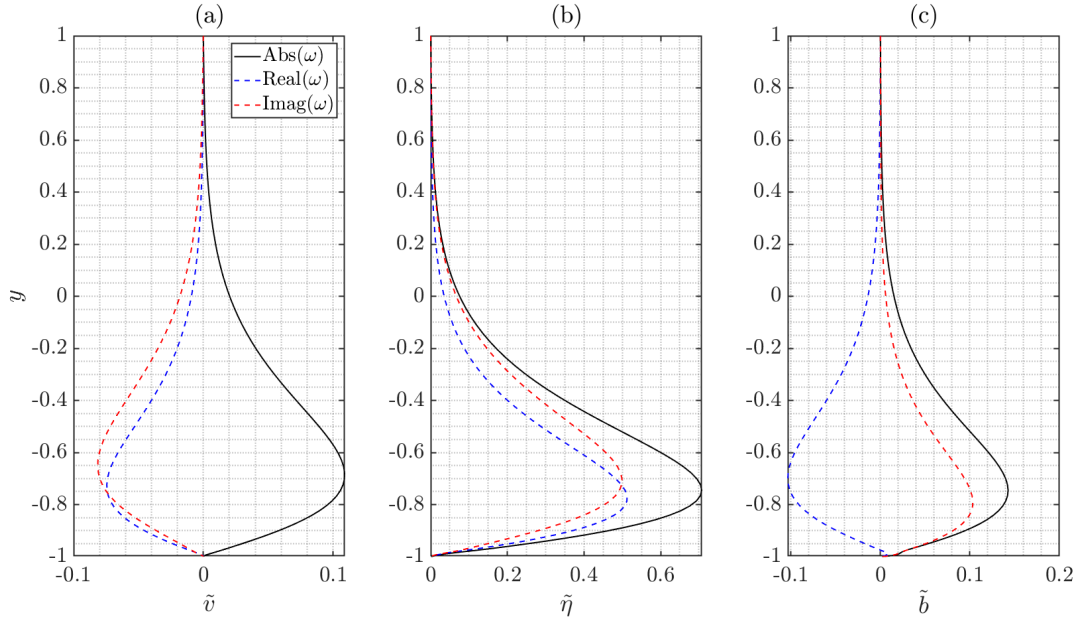

Figure 7.12: Eigenfunctions of the most unstable eigenmode with input parameters $(\alpha, \beta, Re, F_h, \theta) = (0.8, 5, 80000, 1, 5)$ for the pCf, where (a) represents the velocity perturbations, (b) wall-normal vorticity perturbations and (c) buoyancy perturbations. Curves refer to the absolute value and real and imaginary parts of ω.

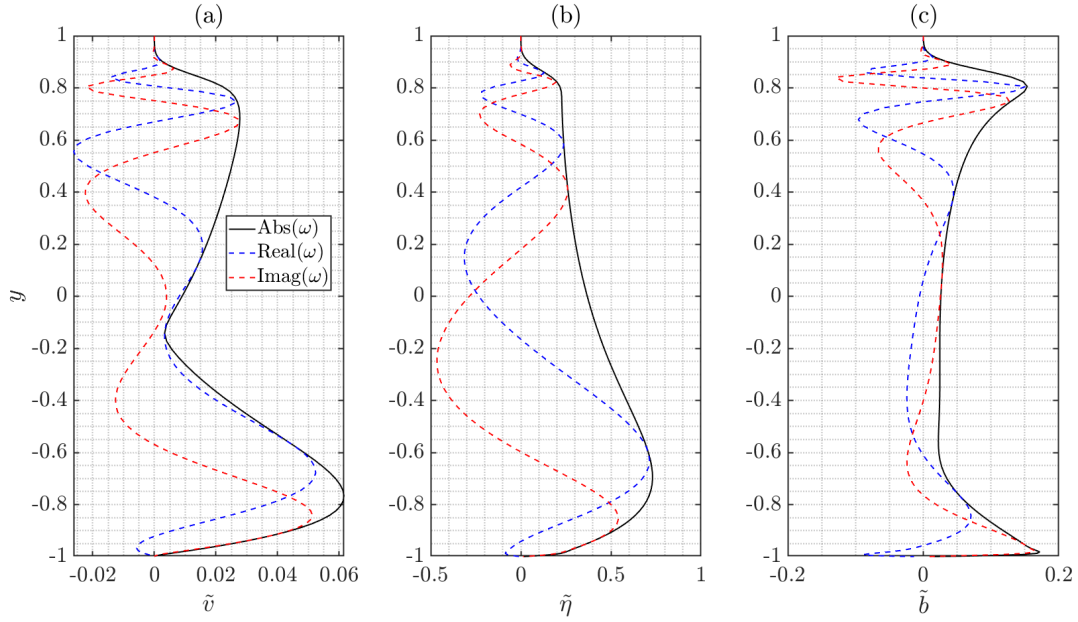

Figure 7.13: Eigenfunctions of the most unstable eigenmode with input parameters $(\alpha, \beta, Re, F_h, \theta) = (0.8, 5, 80000, 1, 60)$ for the pCf flow, where (a) represents the velocity perturbations, (b) wall-normal vorticity perturbations and (c) buoyancy perturbations. Curves refer to the absolute value and real and imaginary parts of ω.

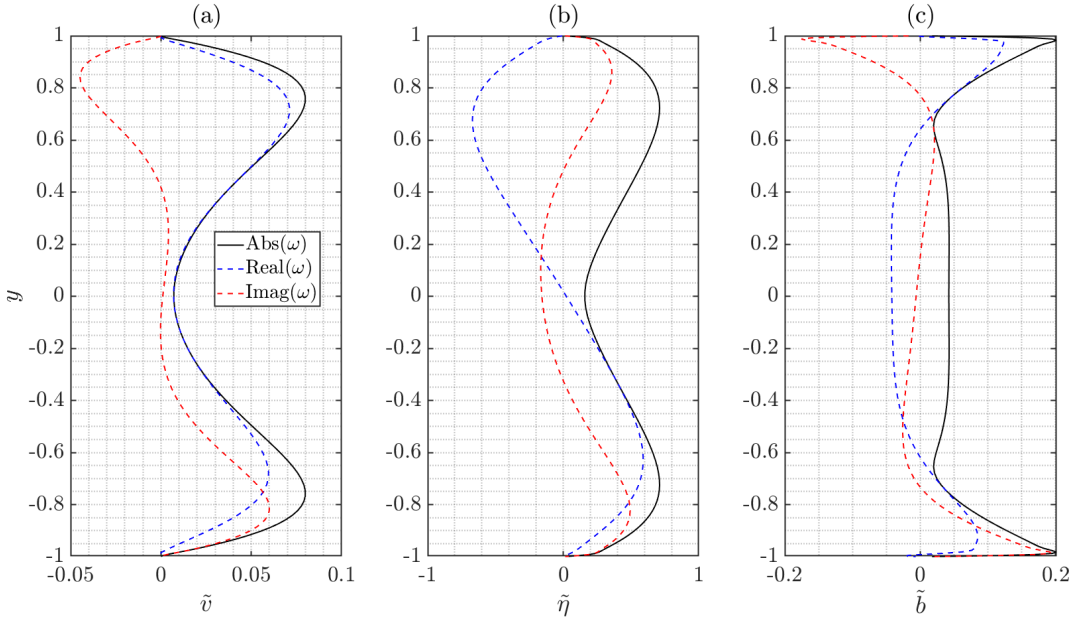

Figure 7.14: Eigenfunctions of the most unstable eigenmode with input parameters $(\alpha, \beta, Re, F_h, \theta) = (0.8, 5, 80000, 1, 80)$ for the pCf flow, where (a) represents the velocity perturbations, (b) wall-normal vorticity perturbations and (c) buoyancy perturbations. Curves refer to the absolute value and real and imaginary parts of ω.

To understand why the asymmetric perturbation profiles appear for lower tilt angles, one can investigate the eigenspectra in these cases. The two most unstable eigenvalues are presented in Table 7.2. Evaluating the values tabulated, one can instantly observe that for the tilt cases lower than 80 degrees, the most unstable eigenmode is actually a conjugate pair. This is consistent with what was found in the eigenspectra plots in Section 7.1, where the most unstable eigenmode coalesces into a single non-oscillatory mode around a tilt angle of 80 degrees. Therefore, one can conclude that modes with stationary eigenmodes are symmetric in the streamnormal direction y, as shown by the case of 80 degrees (Figure 7.14). Conversely, oscillatory modes with a conjugate pair of the most unstable eigenmode exhibit asymmetric profiles. To reinforce this finding, plots of the eigenfunctions of the conjugate pair eigenmodes are produced for tilt cases 5 and 60 degrees, as shown in Figures 7.15 and 7.16. These plots exhibit identical shapes to their conjugate pair eigenfunctions, thus allowing the conclusion that the conjugate pair oscillatory unstable modes produce asymmetric perturbation profiles with the conjugate pair profile being the y-mirror of the other with respect to $y = 0$.

Table 7.2: Two most unstable eigenmodes for the tilt angles shown in the eigenfunction plots. Note that the complex frequency, $\omega = \omega_r + i\omega_i$, is tabulated.

θ [deg]	ω_{max}	ω_{max-1}
5	-1.3439 - 0.0030i	1.3439 - 0.0030i
60	-0.1417 + 0.0116i	0.1417 + 0.0116i
80	0.0000 + 0.0129i	0.1736 - 0.0102i

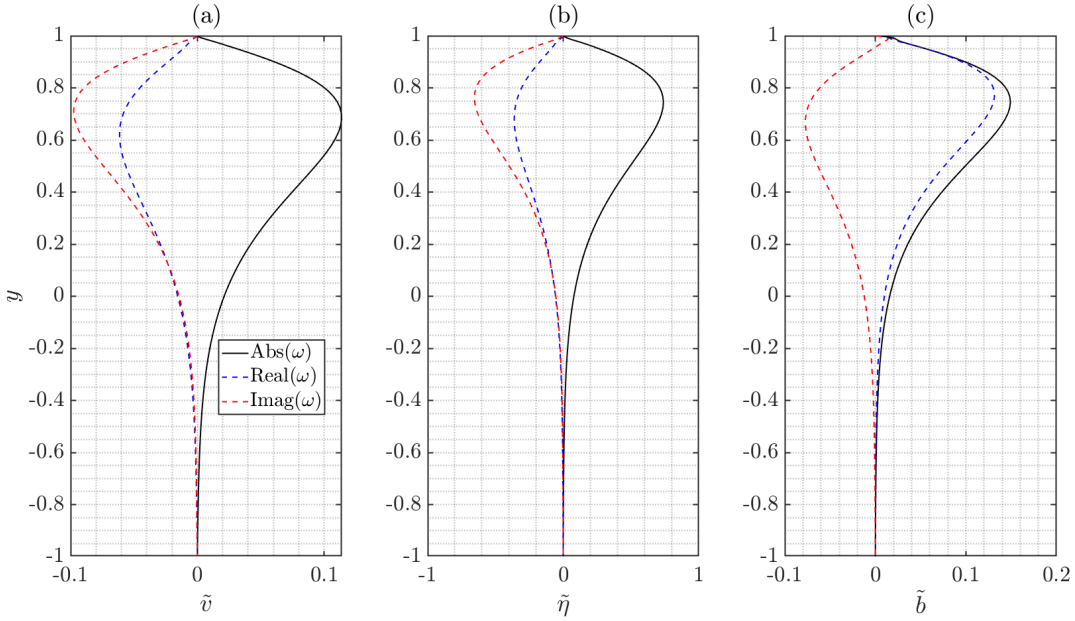

Figure 7.15: Eigenfunctions of the most unstable eigenmode with the conjugate pair, input parameters consistent with Figure 7.12, for the pCf, where (a) represents the velocity perturbations, (b) wall-normal vorticity perturbations and (c) buoyancy perturbations. Curves refer to the absolute value and real and imaginary parts of ω.

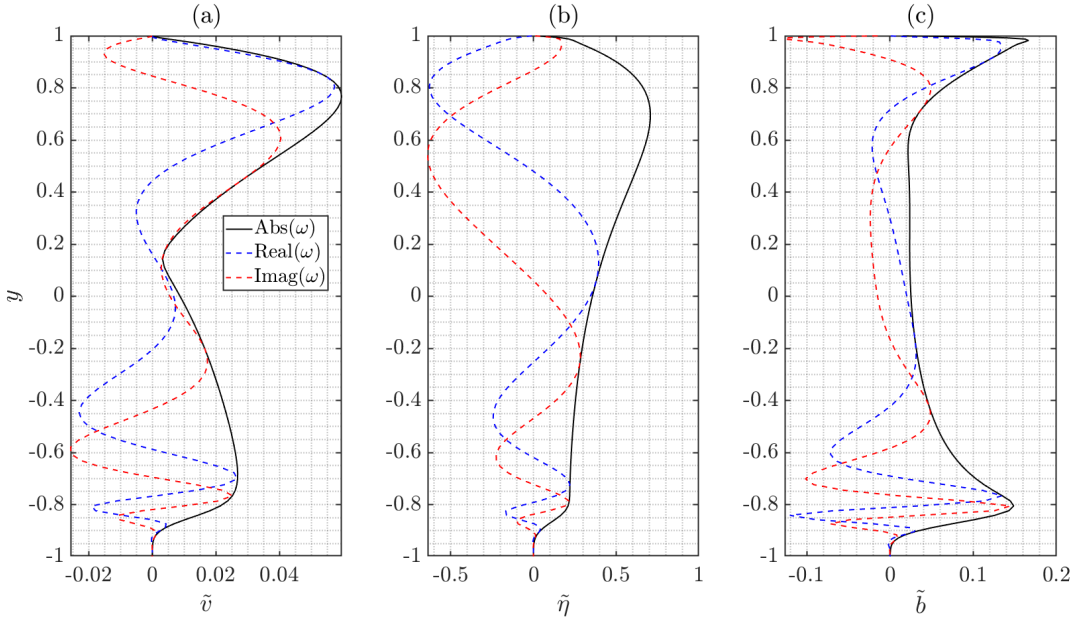

Figure 7.16: Eigenfunctions of the most unstable eigenmode with the conjugate pair, input parameters consistent with Figure 7.13, for the pCf, where (a) represents the velocity perturbations, (b) wall-normal vorticity perturbations and (c) buoyancy perturbations. Curves refer to the absolute value and real and imaginary parts of ω.

Complete confirmation of this deduction can be observed by the eigenfunction plots of the pPf shown in Appendix D. Note that in Section 7.1, the eigenspectra for the pPf always produced a single unstable eigenmode thus the eigenfunction profiles are all symmetric in the shear planes with respect to $y = 0$. This symmetry result is similar to what was found in Facchini [1] and Satomura [14]. Figure 6 of Satomura analysed the stability of non-stratified pCf in the shallow-water approximation. This author suggested that the non-oscillatory instability was produced by the resonance of two Doppler-shifted waves. More recently, the same mechanism was reported to be responsible for linear stratified instabilities producing symmetrical perturbations for Taylor-Couette flows [15]. This is a fairly premature conclusion and is assuming the same mechanism is responsible for the apparent symmetrical perturbation profiles. Deeper analysis into this potential mechanism is required.

To account for the conjugate pair of unstable eigenmodes for the pCf, the Solver was updated. The Solver now checks wheteher the most unstable eigenmode is in fact a conjugate pair. In the scenario this result is found, the user is informed through a command window display shown in Figure C.3 in Appendix C.2, and then, should the user request plots of the figures, both eigenfunction profiles of the conjugate pair will be produced.

7.7 Effect Of Schmid Number, Sc

As mentioned in the introduction to this chapter, the Sc was held constant at a value of 700. This is the value that the Sc typically takes in all major research. Facchini [1] carried out analysis on the consequence of changing its value. Sc was plotted for values of 1, 7, 700 and ∞. Setting Sc in the limit $Sc \to \infty$ is the case where mass diffusivity was completely neglected. Facchini concludes that its value is not important, provided $Sc \geq 7$.

Chapter 8

Conclusions and Future Work

In this report, the presented work has reviewed the theory of Hydrodynamic Stability, in particular Linear Stability Analysis, and how these theories can be applied to stratified flows. Past works on stratification were discussed for a variety of shear flows. The well understood result was that stable stratification has a stabilising effect to the shear flow when the shear and stratification are aligned.

Introducing an unalignment between the stratification and shear planes was a key feature in unlocking a complete understanding of the linear stability of stratified shear flows. A particular interest was shown in adopting the Orr-Sommerfeld and Squire theorem to solving the stratified system. To this end, a detailed description of the derivation of the stratified shear system was included by closely following the Orr-Sommerfeld/Squire system. An implementation of a MATLAB Solver was performed to carry out the LSA of a tilted stratified plane to a plane shear flow (pCf and pPf shear profiles were presented here) and output the growth rate and perturbation shapes under certain conditions set by $(\alpha, \beta, Re, F_h, \theta)$. The Solver utilised the Chebyshev Transform Method to numerically represent the perturbation profiles of the reduced state variables $(\tilde{v}, \tilde{\eta}, \tilde{b})$, where the number of grid points, N, could be set by the user. Convergence analysis was carried out to determine a compromise between computational cost and accuracy which showed that $N = 100$ was an appropriate value to take forward, which was consistent with past works. With the rich volume of existing research, validation of the Solver was extensively performed to reinforce the correctness of the produced results. This was mainly carried out using Facchini [1] and Schmid and Henningson [10]. The script was proven to be both flexible and robust to adopt both unstratified and stratified governing equations while solving the linearised equations accurately.

After complete development of the function `OS_SQ_Stratified_Solver.m`, this Solver could be utilised to furthering an understanding on the influences a tilted stratification has on the stabilisation of plane shear flows. The fundamental assumptions of incompressible flows with a linear density gradient from the gravity of the stratification plane and impenetrable/no-slip conditions were applied to the shear plane walls. Moreover, Dirichlet boundary conditions were imposed after careful evaluation of past works. The Solver was employed to firstly investigate the features of unaligned stratified shear stability by varying the governing input parameters $(\alpha, \beta, Re, F_h, \theta)$. Key results found that instabilities are induced at wavenumbers $(\alpha, \beta) = (0.8, 5)$ for the pCf and $(\alpha, \beta) = (1.5, 6)$ for the pPf. When raising the tilt angle from 0 degrees towards 90 degrees, it was found how the critical Reynolds number exhibited exponential decay for both the pCf and pPf. Moreover, despite the expected stabilising effect of increasing the stratification strength, it was found that, when tilted, there existed a region where increasing the stratification strength has a destabilising effect, which was defined as the destabilisation zone. Finally, in general, increasing the tilt angle had a destabilising effect. In the pCf case, as the tilt is raised, the growth rate of the most unstable

eigenmode becomes more positive. This mode has a conjugate pair and as the tilt is increased, the two most unstable modes move closer together and between 60 to 80 degrees, the pair coalsce to form a single non-oscillatory eigenmode.

8.1 Future Work

This report does not present a complete understanding to the physics behind the instabilities produced from unaligning the stratification to the shear. To build towards this the following work can be performed to complete the picture of stratified shear stability.

Non-linear analysis of the governing system of equations could be carried out, the results of which could be compared with the LSA presented here and determine whether important features of instability were missed from the linearised approximation. Lucas [3] found that implementation of the buoyancy boundary conditions were flexible to either the no flux or Dirichlet conditions. To confirm this, the Solver could be edited to implement Neumann conditions. Moreover, to build on the discussions presented here, a more complete analysis of the pPf could be performed and potentially extended to other shear flows. A more complete understanding of the flow physics could be carried out to confirm why the features of instabilities are observed under certain conditions. In particular, this would be interesting for the destabilisation zone in decreasing F_h. To this end, the critical Froude number, defined as the point of which the destabilisation consequence begins, could be investigated for a larger array of unalignment angles. Finally, the proposed Doppler-shift mechanism for the single unstable eigenmode requires further analysis to valid this finding.

Bibliography

[1] Giulio Facchini, Benjamin Favier, Patrice Le Gal, Meng Wang, and Michael Le Bars. The linear instability of the stratified plane couette flow. *Journal of Fluid Mechanics*, 853:205–234, 2018.

[2] Julien Candelier, Stéphane Le Dizès, and Christophe Millet. Shear instability in a stratified fluid when shear and stratification are not aligned. *Journal of fluid mechanics*, 685:191–201, 2011.

[3] Dan Lucas, CP Caulfield, and Rich R Kerswell. Layer formation and relaminarisation in plane couette flow with spanwise stratification. *Journal of Fluid Mechanics*, 868:97–118, 2019.

[4] Anubhab Roy and Rama Govindarajan. An introduction to hydrodynamic stability. In *Rheology of Complex Fluids*, pages 131–147. Springer, 2010.

[5] Philippe-Emmanuel P-E Roche. Applicability of boussinesq approximation in a turbulent fluid with constant properties. *arXiv preprint arXiv:0710.3497*, 2007.

[6] Paul Billant and Jean-Marc Chomaz. Self-similarity of strongly stratified inviscid flows. *Physics of fluids*, 13(6):1645–1651, 2001.

[7] Axel Deloncle, Jean-Marc Chomaz, and Paul Billant. Three-dimensional stability of a horizontally sheared flow in a stably stratified fluid. *Journal of Fluid Mechanics*, 570:297–305, 2007.

[8] Steven A Orszag. Accurate solution of the orr–sommerfeld stability equation. *Journal of Fluid Mechanics*, 50(4):689–703, 1971.

[9] Lloyd Fung and Yongyun Hwang. Linear instability of tilted parallel shear flow in a strongly stratified and viscous medium.

[10] Peter J Schmid, Dan S Henningson, and DF Jankowski. Stability and transition in shear flows. applied mathematical sciences, vol. 142. *Appl. Mech. Rev.*, 55(3):B57–B59, 2002.

[11] Parviz Moin. *Fundamentals of engineering numerical analysis*. Cambridge University Press, 2010.

[12] Rob-Roy L Mace. Reduction of the gibbs phenomenon via interpolation using chebyshev polynomials, filtering and chebyshev-pade'approximations. 2005.

[13] J Andre Weideman and Satish C Reddy. A matlab differentiation matrix suite. *ACM Transactions on Mathematical Software (TOMS)*, 26(4):465–519, 2000.

[14] Takehiko Satomura. An investigation of shear instability in a shallow water. *Journal of the Meteorological Society of Japan. Ser. II*, 59(1):148–167, 1981.

[15] Junho Park and Paul Billant. The stably stratified taylor–couette flow is always unstable except for solid-body rotation. *Journal of Fluid Mechanics*, 725:262–280, 2013.

Appendix A

Stratified System Derivation

In this Chapter, the full derivation of the stratified Orr-Sommerfeld/Squire system shall be presented. The full manipulations that were performed to the linearised governing equations will be shown for clarity of how the final system of equations were reached. Note that the derivation largely follows the steps employed by the famous Orr-Sommerfeld and Squire system.

A.1 Velocity Form

There is an interest in finding a time derivative for the streamnormal velocity perturbation, v', as a function of the reduced state variables, $f(\frac{\partial v'}{\partial t}, v', \eta', b') = 0$, which is the velocity form of the system. It is useful to remove the influence of the streamwise and spanwise velocity components. In order to find the velocity form, one most follow the preceding manipulation; $\frac{\partial}{\partial x}$(5.1.9a), $\frac{\partial}{\partial y}$(5.1.9b), $\frac{\partial}{\partial z}$(5.1.9c) to the linearised momentum equations. The outcome is presented below:

$$\frac{\partial}{\partial t}\left(\frac{\partial u'}{\partial x}\right) + \frac{\partial}{\partial x}\left(U\frac{\partial u'}{\partial x}\right) + \frac{\partial}{\partial x}\left(v'\frac{dU}{dy}\right) = -\frac{\partial^2 p'}{\partial x^2} + \frac{1}{Re}\frac{\partial}{\partial x}(\nabla^2 u') \tag{A.1.1a}$$

$$\frac{\partial}{\partial t}\left(\frac{\partial v'}{\partial y}\right) + \frac{\partial}{\partial y}\left(U\frac{\partial v'}{\partial x}\right) = -\frac{\partial^2 p'}{\partial y^2} + \frac{1}{Re}\frac{\partial}{\partial y}(\nabla^2 v') - \frac{1}{F_h^2}\frac{\partial b'}{\partial y}\cos\theta \tag{A.1.1b}$$

$$\frac{\partial}{\partial t}\left(\frac{\partial w'}{\partial z}\right) + \frac{\partial}{\partial z}\left(U\frac{\partial w'}{\partial x}\right) = -\frac{\partial^2 p'}{\partial z^2} + \frac{1}{Re}\frac{\partial}{\partial z}(\nabla^2 w') + \frac{1}{F_h^2}\frac{\partial b'}{\partial z}\sin\theta \tag{A.1.1c}$$

Next we sum Equations (A.1.1a), (A.1.1b) and (A.1.1c) and applying the linearised continuity, Equation (5.1.10), one finds:

$$\begin{aligned}
&\frac{\partial}{\partial t}\left(\cancel{\frac{\partial u'}{\partial x}} + \cancel{\frac{\partial v'}{\partial y}} + \cancel{\frac{\partial w'}{\partial z}}\right) + U\frac{\partial}{\partial x}\left(\cancel{\frac{\partial u'}{\partial x}} + \cancel{\frac{\partial v'}{\partial y}} + \cancel{\frac{\partial w'}{\partial z}}\right) + 2\frac{dU}{dy}\frac{\partial v'}{\partial x} \\
&= -\nabla^2 p' + \frac{1}{Re}\left(\frac{\partial^2}{\partial x^2}\left(\cancel{\frac{\partial u'}{\partial x}} + \cancel{\frac{\partial v'}{\partial y}} + \cancel{\frac{\partial w'}{\partial z}}\right) + \frac{\partial^2}{\partial y^2}\left(\cancel{\frac{\partial u'}{\partial x}} + \cancel{\frac{\partial v'}{\partial y}} + \cancel{\frac{\partial w'}{\partial z}}\right) + \frac{\partial^2}{\partial z^2}\left(\cancel{\frac{\partial u'}{\partial x}} + \cancel{\frac{\partial v'}{\partial y}} + \cancel{\frac{\partial w'}{\partial z}}\right)\right) \\
&+ \frac{1}{F_h^2}\frac{\partial b'}{\partial z}\sin\theta - \frac{1}{F_h^2}\frac{\partial b'}{\partial y}\cos\theta
\end{aligned} \tag{A.1.2}$$

This leaves the stratified form of the Poisson equation for pressure, shown in Equation (A.1.3) below.

$$\nabla^2 p' = -2\frac{dU}{dy}\frac{\partial v'}{\partial x} + \frac{1}{F_h^2}\frac{\partial b'}{\partial z}\sin\theta - \frac{1}{F_h^2}\frac{\partial b'}{\partial y}\cos\theta \tag{A.1.3}$$

Now, elimination the pressure term is performed. By just looking at Equation (5.1.9b) and the stratified Poisson equation for pressure, one can carry out; ∇^2(5.1.9b) and $\frac{\partial}{\partial y}$(A.1.3), which gives:

$$\nabla^2\left(\frac{\partial v'}{\partial t} + U\frac{\partial v'}{\partial x}\right) = -\frac{\partial}{\partial y}\nabla^2 p' + \frac{1}{Re}\nabla^4 v' - \frac{1}{F_h^2}\nabla^2 b'\cos\theta \tag{A.1.4a}$$

$$-\frac{\partial}{\partial y}\nabla^2 p' = 2\frac{\partial}{\partial y}\left(\frac{dU}{dy}\frac{\partial v'}{\partial x}\right) - \frac{1}{F_h^2}\frac{\partial^2 b'}{\partial y \partial z}\sin\theta + \frac{1}{F_h^2}\frac{\partial^2 b'}{\partial y^2}\cos\theta \tag{A.1.4b}$$

Equating the pressure terms together:

$$\nabla^2\left(\frac{\partial v'}{\partial t} + U\frac{\partial v'}{\partial x}\right) - \frac{1}{Re}\nabla^4 v' + \frac{1}{F_h^2}\nabla^2 b'\cos\theta = 2\frac{\partial}{\partial y}\left(\frac{dU}{dy}\frac{\partial v'}{\partial x}\right) - \frac{1}{F_h^2}\frac{\partial^2 b'}{\partial y \partial z}\sin\theta + \frac{1}{F_h^2}\frac{\partial^2 b'}{\partial y^2}\cos\theta \tag{A.1.5}$$

Now looking at second term in Equation (A.1.5), it can be simplified to:

$$\nabla^2\left(U\frac{\partial v'}{\partial x}\right) = U\frac{\partial}{\partial x}\left(\nabla^2 v'\right) + \frac{d^2U}{dy^2}\frac{\partial v'}{\partial x} + 2\frac{dU}{dy}\frac{\partial^2 v'}{\partial x \partial y} \tag{A.1.6}$$

Finally putting Equation (A.1.6) back into Equation (A.1.5) and rearranging one comes to the final velocity form:

$$\left[\left(\frac{\partial}{\partial t} + U\frac{\partial}{\partial x}\right)\nabla^2 - \frac{d^2U}{dy^2}\frac{\partial}{\partial x} - \frac{1}{Re}\nabla^4\right]v' + \left[\frac{1}{F_h^2}\left(\nabla^2\cos\theta - \frac{\partial^2}{\partial y^2}\cos\theta + \frac{\partial^2}{\partial y \partial z}\sin\theta\right)\right]b' = 0 \tag{A.1.7}$$

A.2 Vorticity Form

Next there is an interested in finding a time derivative for the wall-normal vorticity perturbation, η', as a function of the reduced state variables, $f(\frac{\partial \eta'}{\partial t}, v', \eta', b') = 0$, which is the vorticity form of the system. Once again, one can manipulate the momentum equations by $\frac{\partial}{\partial x}$(5.1.9c) and $\frac{\partial}{\partial z}$(5.1.9a).

$$\frac{\partial}{\partial t}\left(\frac{\partial u'}{\partial z}\right) + U\frac{\partial^2 u'}{\partial x \partial z} + \frac{dU}{dy}\frac{\partial v'}{\partial z} = -\frac{\partial^2 p'}{\partial x \partial z} + \frac{1}{Re}\frac{\partial}{\partial z}\left(\nabla^2 u'\right) \tag{A.2.1a}$$

$$\frac{\partial}{\partial t}\left(\frac{\partial w'}{\partial x}\right) + U\frac{\partial^2 w'}{\partial x^2} = -\frac{\partial^2 p'}{\partial x \partial z} + \frac{1}{Re}\frac{\partial}{\partial x}\left(\nabla^2 w'\right) + \frac{1}{F_h^2}\frac{\partial b'}{\partial x}\sin\theta \tag{A.2.1b}$$

Finally subtracting Equation (A.2.1b) from Equation (A.2.1a) and substituting $\eta' = \left(\frac{\partial u'}{\partial z} - \frac{\partial w'}{\partial x}\right)$ will give the stratified Squire system:

$$\left[\frac{\partial}{\partial t} + U\frac{\partial}{\partial x} - \frac{1}{Re}\nabla^2\right]\eta' + \left[\frac{dU}{dy}\frac{\partial}{\partial z}\right]v' + \left[\frac{1}{F_h^2}\frac{\partial}{\partial x}\sin\theta\right]b' = 0 \tag{A.2.2}$$

A.3 Density Transport Form

Finally, there is an interested in finding the last time derivative equation of the final stratified system for the dimensionless buoyancy perturbation, b', as a function of the reduced state variables, $f(\frac{\partial b'}{\partial t}, v', \eta', b') = 0$, which is the density transport form of the system. Subbing in that $Y = y\cos\theta - z\sin\theta$, the linearised density transport gives:

$$\left[\frac{\partial}{\partial t} + U\frac{\partial}{\partial x} - \frac{1}{ReSc}\nabla^2\right]b' - \left[\frac{\cos\theta}{F_h^2}\right]v' + \left[\frac{\sin\theta}{F_h^2}\right]w' = 0 \tag{A.3.1}$$

A.3.1 $\tilde{w} = f(\tilde{v}, \tilde{\eta})$

The wall-normal vorticity can be written in normal-mode form:

$$\tilde{\eta} = (\frac{\partial \tilde{u}}{\partial z} - \frac{\partial \tilde{w}}{\partial x}) = i\beta\tilde{u} - i\alpha\tilde{w} \tag{A.3.2}$$

Also, the same is performed with the linearised continuity equation:

$$i\alpha\tilde{u} + \mathcal{D}\tilde{v} + i\beta\tilde{w} = 0 \tag{A.3.3}$$

Rearranging the continuity equation in terms of $\tilde{u} = \frac{i}{\alpha}(\mathcal{D}\tilde{v} + i\beta\tilde{w})$ and substituting this into Equation (A.3.2), one finds $\tilde{w} = f(\tilde{v}, \tilde{\eta})$:

$$\tilde{w} = \frac{1}{k^2}\big(i\beta\mathcal{D}\tilde{v} + i\alpha\tilde{\eta}\big) \tag{A.3.4}$$

Appendix B

Discrete Chebyshev Transform Method

A more detailed description of the numerical method is presented here for completeness and to provide an understanding of how the implementation was carried out. An arbitrary smooth function can be represented in terms of a series of orthogonal polynomials, which are the eigenfunctions. An advantage of using polynomial expansions to approximate arbitrary functions is their superior resolution capabilities near boundaries. The arbitrary smooth function, $u(x)$, defined in the domain $-1 \leq x \leq 1$, is approximated by the finite series of Chebyshev polynomials:

$$u(x) = \sum_{n=0}^{N} a_n T_n(x), \tag{B.0.1}$$

where n represents the polynomial order, N is the finite highest order polynomial and a_n are the Chebshev coefficients with $T_n(x)$ representing the Chebyshev polynomals of order n.

The Chebyshev polynomials are solutions of the differential eigenvalue problem:

$$\frac{d}{dx}\left(\sqrt{1-x^2}\frac{dT_n}{dx} + \frac{\lambda_n}{\sqrt{1-x^2}}T_n\right) = 0 \tag{B.0.2}$$

where $\lambda_n = n^2$ are the eigenvalues. The first few Chebyshev polynomials are $T_0 = 1$, $T_1 = x$, $T_2 = 2x^2 - 1$ and so on. A key property of the Chebyshev polynomials is that they become simple cosines with the transformation of the independent variable $x = \cos\theta$, which maps $1 \leq x \leq 1$ into $0 \leq \theta \leq \pi$. The transformation is:

$$T_n(\cos\theta) = \cos n\theta. \tag{B.0.3}$$

This is a useful feature of Chebyshev polynomial expansions as the representation is reverted to cosine transforms and in the discrete case one can take advantage of the First Fourier Transform algorithm. Exploiting trigonometry, the following recursive relation can be used to generate $T_n(x)$:

$$T_{n+1}(x) + T_{n-1}(x) = 2xT_n(x) \qquad b \leq 1. \tag{B.0.4}$$

Other important properties of Chebyshev polynomials are listed below:

- $|T_n(x)| \leq 1$ in domain $-1 \leq x \leq 1$
- $T_n(\pm 1) = (\pm 1)^n$.

For numerical analysis, the domain is discretised using a cosine mesh:

$$x_j = \cos\frac{\pi j}{N} \qquad j = N, N-1, ..., 1, 0. \tag{B.0.5}$$

The discrete Chebyshev transform representation of u on a discrete set of points is defined as:

$$u_j = \sum_{n=0}^{N} a_n T_n(x_j) = \sum_{n=0}^{N} a_n \cos\frac{n\pi j}{N} \qquad j = 0, 1, 2, ..., N \tag{B.0.6}$$

Note that the Chebyshev coefficients are determined from:

$$a_n = \frac{2}{c_n N} \sum_{j=0}^{N} \frac{1}{c_j} u_j T_n(x_j) = \frac{2}{c_n N} \sum_{j=0}^{N} \frac{1}{c_j} u_j \cos\frac{n\pi j}{N} \tag{B.0.7}$$

where $n = 0, 1, 2, ..., N$ and c_n is determined by:

$$c_n = \begin{cases} 2 & \text{if } n = 0, N \\ 1 & \text{otherwise.} \end{cases} \tag{B.0.8}$$

The next step is to develop the relationship between the Chebyshev coefficients of the function and its derivatives:

$$u'(x) = \sum_{n=0}^{N-1} b_n T_n(x) \tag{B.0.9}$$

where b_n are the derivative coefficients and note that the derivative polynomial is of order $N-1$. One can differentiate Equation (B.0.1) and equate it to Equation (B.0.9). After some manipulation as shown in [11], the relation between a_n and b_n can be found from:

$$c_{n-1} b_{n-1} - b_{n+1} = 2n a_n \qquad n = 1, 2, ..., N \tag{B.0.10}$$

where $b_N = b_{N+1} = 0$. In summary to compute the derivative of a function u, firstly compute its Chebyshev coefficients using Equation (B.0.7), then the derivative coefficients can be obtained from Equation (B.0.10). The derivative function can then be represented by Equation (B.0.9). As a final comment one can express the Chebyshev derivatives in matrix form and this was what was implemented in the code. Hence all derivatives in the y-direction, $\mathcal{D}, \mathcal{D}^2$ and $\mathcal{D}^4$ were approximated by a matrix of Chebyshev coefficients.

Appendix C

Stratified System Solver

The presentation of the developed Statified Orr-Sommerfeld Squire Solver using MATLAB is found in this chapter. Firstly, the code infrastructure is introduced, followed by the main outputs that are displayed to the user for clarity and finally the full MATLAB program. The program consists of a main function which ultilises secondary functions, and various simulations of different input conditions can be run in the main MATLAB program. Complete validation of the Chebyshev grid point convergence and comparison with Facchini [1] is also shown.

C.1 Code Infrastructure

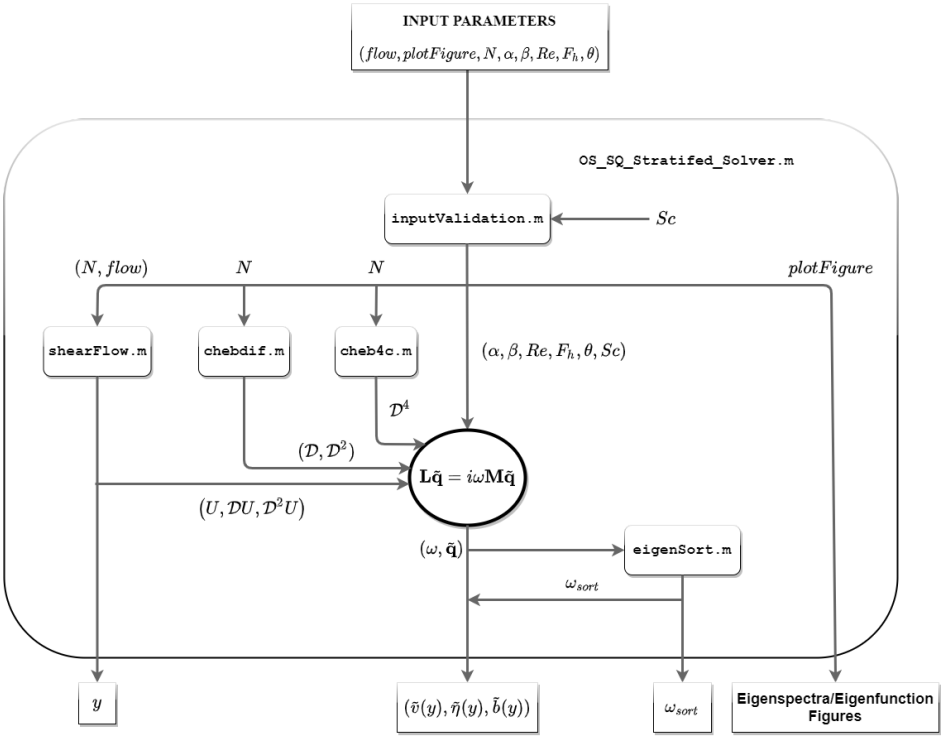

Figure C.1: MATLAB Solver infrastructure to visual the steps involved to perform the Linear Stability Analysis of stratified shear flows.

C.2 Code Output Window

```
================================================================
          LINEAR STABLILTY ANALYSIS OF AN INALIGNED
         DENSITY STRATIFICATION TO A PLANE SHEAR FLOW
================================================================
---------------------- INPUT PARAMETERS ----------------------
User Inputs:
flow:          plane Couette flow
plotFigure:    Eigenspectra/Eigenfunctions to be plotted
N:             100
alpha:         0.800
beta:          5.000
Re:            1000.000
Fh:            1.000
theta:         60.000 degrees

Constant parameter:
Sc:             700.000

Velocity profile:              Density profile:
(x,y) plane                    (X,Y) plane
===================            ======================
          -------->            --->
          ------>              ----->
          ---->                ------->
          -->                  --------->
          >                    ---------->
         <                     ---------->
       <--                     ---------->
     <----                     ---------->
   <------                     ---------->
 <--------                     ---------->
===================            ======================
----------------------------------------------------------------
```

Figure C.2: Command window output from running the main MATLAB solver, the function displays the user inputs and the density and velocity profiles to optimise the usability and clarity of the solver.

```
------------------------ Information -------------------------
       The most unstable eigenmode has a conjugate pair
      Eigenfunctions of both eigenmodes will be plotted
----------------------------------------------------------------
```

Figure C.3: Command window output in the scenario when the most unstable eigenmode has a conjugate pair to maximise clarity.

C.3 MATLAB Program

Listing C.1: `OS_SQ_Stratified_Analysis.m`

```
1
2  % ====================== INTRODUCTION TO PROGRAM ==========================
3  %
4  % Program to run different test cases of the Orr-Sommerfeld (OS) and Squire
5  % (SQ) Stratified Solver function: OS_SQ_Stratified_Solver.m
6  % Used to produce useful results and plots for analysis of the statiblity
7  % of an inaligned density stratification to a plane shear flow
8  %
9  % ====================== Main parameter inputs ============================
10 %
11 % OS_SQ_Stratified_Solver.m function:
12 %
13 % INPUTS:
14 % ( 1 ) Chosen shear flow ( pCf = 1; pPf = 2 ) [ flow ]
15 % ( 2 ) Request whether to produce plots ( Yes = 1; No = 0 ) [ plotFigure ]
16 % ( 3 ) Number of Chebyshev grid points [ N ]
17 % ( 4 ) Wavenumber ( x-direction ) [ alpha ]
18 % ( 5 ) Wavenumber ( z-direction ) [ beta ]
19 % ( 6 ) Reynold number [ Re ]
20 % ( 7 ) Froude number ( horizontal ) [ Fh ]
21 % ( 8 ) Shear/stratification inalignment angle [ theta ] ( degrees )
22 %
23 % OUTPUTS:
24 % ( 1 ) Complex frequency sorted by the growth rate from least stable
25 % eigenmodes to most stable [ omega_stratSort ]
26 % ( 2 ) Eigenfunctions of the most unstable eigenmode [ eFunction ]
27 % ( 3 ) Domain grid points between -1 to 1 [ ymesh ]
28
29 % --------------------------- BEGIN PROGRAM -----------------------------
30
31 clear
32 clc
33 close all
34
35 % Example input parameters
36 pCf = 1;
37 pPf = 2;
38 plotFigure = 1;
39 N = 100;
40 alpha = 1;
41 beta = 0;
42 Re = 1000;
43 Fh = 1;
44 theta = 30;
```

```
45
46 % Example simulation for pCf
47 [omega_pCf,eFunction_pCf,ymesh_pCf] =
       OS_SQ_Stratified_Solver(pCf,plotFigure,N,alpha,beta,Re,Fh,theta);
48
49 % Example simulation for pPf
50 [omega_pPf,eFunction_pPf,ymesh_pPf] =
       OS_SQ_Stratified_Solver(pPf,plotFigure,N,alpha,beta,Re,Fh,theta);
51
52 %---------------------------- END OF PROGRAM -----------------------------
```

Listing C.2: `OS_SQ_Stratified_Solver.m`

```
1  function [omega_stratSort,eFunction,ymesh] =
       OS_SQ_Stratified_Solver(flow,plotFigure,N,alpha,beta,Re,Fh,theta)
2
3      % ==================== INTRODUCTION TO FUNCTION ======================
4      %
5      % Linear Stability Analysis of a density stratified plane shear flow
6      % with a linear stratification and shear inalignment by angle theta
7      %
8      % Shear flows:
9      % pCf - plane Couette flow
10     % pPf - plane Poiseuille flow
11     %
12     % Edited by: Joel Outschoorn
13     % {Ref 1}: Outschoorn; Transition In Stratified Shear Flows: Linear
14     % Stability Analysis With A Shear And Stratification Inalignment
15     %
16     % {Ref 2}: Schmid and Henningson; Stability and Transition in Shear Flows
17     %
18     % ====================== Main user inputs ============================
19     %
20     % INPUTS:
21     % ( 1 ) Chosen shear flow ( pCf = 1; pPf = 2 ) [ flow ]
22     % ( 2 ) Request whether to produce plots ( Yes = 1; No = 0 ) [ plotFigure ]
23     % ( 3 ) Number of Chebyshev grid points [ N ]
24     % ( 4 ) Wavenumber ( x-direction ) [ alpha ]
25     % ( 5 ) Wavenumber ( z-direction ) [ beta ]
26     % ( 6 ) Reynold number [ Re ]
27     % ( 7 ) Froude number ( horizontal ) [ Fh ]
28     % ( 8 ) Shear/stratification inalignment angle [ theta ] ( degrees )
29     %
30     % OUTPUTS:
31     % ( 1 ) Complex frequency sorted by the growth rate from least stable
32     % eigenmodes to most stable [ omega_stratSort ]
33     % ( 2 ) Eigenfunctions of the most unstable eigenmode [ eFunction ]
34     % ( 3 ) Domain grid points between -1 to 1 [ ymesh ]
```

```
35    %
36    % ================= Governing eigenvalue problem ======================
37    %
38    % Eigenvalue problem - Equations (5.23) and (5.24) in {Ref 1}
39    %
40    % L_strat*q_strat = c_strat*M_strat*q_strat
41    %
42    % L_strat = [ Los, zeros, Losb;
43    % zi*beta*DU, Lsq, zi*alpha*sind(theta);
44    % Lv, (sind(theta)/(Fh^2*k2))*zi*alpha, Lb ];
45    %
46    % M_strat = [(k2*I - D2), zeros, zeros;
47    % zeros, eye, zeros;
48    % zeros, zeros, eye ];
49    %
50    % q_strat = [v_tilde eta_tilde b_tilde]
51    %
52    % c_strat -> eigenvalue
53    % c_strat = i*omega_strat -> omega_strat = -i*c_strat
54    % omega_strat is the growth rate
55    %
56    % ================ Unstratified system (reference) ====================
57    %
58    % Unstratified System - Equations (3.33) - (3.35) in {Ref 2}
59    %
60    % Orr-Somm
61    % M_os = (k2*I - D2)
62    % L_os = Los
63    %
64    % Orr-Somm and Squire
65    % M = [(k2*I - D2), zeros; zeros, eye]
66    % L = [ Los, zeros; zi*beta*DU, Lsq]
67    %
68    % ======================== Velocity parameters ========================
69    %
70    % Velocity profile U
71    % Velocity gradient DU
72    % Second velocity derivative DDU
73    % pCf - linear velocity profile between -1 to 1
74    % pPf - parabolic velocity profile with no slip at each boundary, max
75    % velocity 1 at the midpoint
76
77    % -------------------------- BEGIN FUNCTION --------------------------
78
79    % Figure formatting
80    set(groot,'defaulttextinterpreter','latex');
81    set(groot, 'defaultAxesTickLabelInterpreter','latex');
82    set(groot, 'defaultLegendInterpreter','latex');
```

```
83
84      % Introduction
85      disp('================================================================')
86      disp(' LINEAR STABLILTY ANALYSIS OF AN INALIGNED ')
87      disp(' DENSITY STRATIFICATION TO A PLANE SHEAR FLOW ')
88      disp('================================================================')
89
90      %-------------------- Validating input parameters ---------------------
91
92      disp('---------------------- INPUT PARAMETERS ----------------------')
93
94      Sc = 700; % Schmid number
95
96      % Validation and displaying value
97      [flow,plotFigure,N,alpha,beta,Re,Fh,theta,Sc] = ...
98          inputValidation(flow,plotFigure,N,alpha,beta,Re,Fh,theta,Sc);
99
100     % Shear flow velocity profile
101     [U,DU,DDU,ymesh] = shearFlow(flow,N);
102
103     % Constants
104     zi = sqrt(-1); % Imaginary number
105     I = eye(N-2); % Identity matrix
106
107     k2 = alpha^2 + beta^2; % k constant
108
109     disp('----------------------------------------------------------------')
110
111     %------------------- Computing Chebyshev derivatives ------------------
112
113     % Functions to compute Chebyshev matrices provided by Dr. Hwang
114     [~, D1] = chebdif(N,1); % Function to compute 1st derivative matrix
115     D1 = D1(2:N-1, 2:N-1); % First derivative ignoring boundaries
116     [~, D2] = chebdif(N,2); % Function to compute 2nd derivative matrix
117     D2 = D2(2:N-1, 2:N-1, 2); % Second derivative ignoring boundaries
118     [~, D4] = cheb4c(N); % Function to compute 4th derivative matrix
119
120     %-------------------- Assembling eigenvalue system --------------------
121
122     % Terms in matrix system, Equations (5.24)
123     Los = zi*alpha*U*(k2*I - D2) + zi*alpha*DDU + (1/Re)*(k2*k2*I - 2*k2*D2 + D4);
124     Losb = (k2*I*cosd(theta) - zi*beta*D1*sind(theta))/(Fh^2);
125     Lsq = zi*alpha*U + (1/Re)*(k2*I - D2);
126     Lv = (sind(theta)/(Fh^2*k2))*zi*beta*D1 - (cosd(theta)/(Fh^2))*I;
127     Lb = (zi*alpha*U + (1/(Re*Sc))*(k2*I - D2))/(Fh^2);
128
129     % Coefficients to L and M matrix
130     ZERO = zeros(N-2);
```

```
131     ONE = eye(N-2);
132
133     % M matrix
134     M_strat = [(k2*I - D2), ZERO, ZERO;
135                ZERO, ONE, ZERO;
136                ZERO, ZERO, ONE ];
137
138     % L matrix
139     L_strat = [ Los, ZERO, Losb;
140                zi*beta*DU, Lsq, (zi*alpha*sind(theta)*I)/(Fh^2);
141                Lv, (sind(theta)/(Fh^2*k2))*zi*alpha*I, Lb ];
142
143     %----------------- Solving and sorting eigenvalues --------------------
144
145     [V,c_strat] = eig(L_strat,M_strat); % System e/spectra and e/functions
146     c_strat = diag(c_strat); % Returning eigenmodes into vector form
147     omega_strat = -zi*c_strat; % Stratified growth rate
148
149     % Sorting e/values from least stable to most stable in terms of the
150     % imaginary part
151     omega_stratSort = eigenSort(omega_strat);
152
153     % Finding eigenfunction for most unstable eigenmode
154     % if statement to find whether most unstable eigenmode has a conjugate
155     % pair
156     if abs(imag(omega_stratSort(1)) - imag(omega_stratSort(2))) < 1e-5
157
158         % Position of most unstable eigenmode in unsorted eigenspectra
159         position1 = find(imag(omega_strat) == imag(omega_stratSort(1)));
160         % Position of most unstable conjugate pair
161         position2 = find(imag(omega_strat) == imag(omega_stratSort(2)));
162
163         % Eigenfunction of the most unstable eigenmode
164         eFunction(:,1) = V(:,position1);
165         % Eigenfunction of the conjugate pair
166         eFunction(:,2) = V(:,position2);
167
168         % Informing the user of the pair of unstable eigenmodes
169         disp('------------------------ Information -------------------------')
170         disp(' The most unstable eigenmode has a conjugate pair ')
171         disp(' Eigenfunctions of both eigenmodes will be plotted ')
172         disp('--------------------------------------------------------------')
173     else
174
175         % Position of most unstable eigenmode in unsorted eigenspectra
176         position = find(imag(omega_strat) == imag(omega_stratSort(1)));
177
178         % Eigenfunction of the most unstable eigenmode
```

```
179         eFunction = V(:,position);
180 
181     end
182 
183     % Plotting eigenspectra and eigenfunction should the user request it
184     if plotFigure == 1
185 
186         % Eigenspectra plot
187         figure
188         plot(omega_stratSort,'kx','Markersize',10,'Linewidth',1.5)
189         hold on
190         % Highlighting the most unstable eigenvalues
191         plot(omega_stratSort(1),'ro','Markersize',15,'Linewidth',1.5)
192         % Conjugate pairs
193         if abs(imag(omega_stratSort(1)) - imag(omega_stratSort(2))) < 1e-5
194             plot(omega_stratSort(2),'ro','Markersize',15,'Linewidth',1.5)
195         end
196         % Highlighting x and y axis
197         plot([-2 2],[0 0],'k-'); plot([0 0],[-2 2],'k-');
198         grid minor; box on; set(gca,'Fontsize',20);
199         ylim([-1 0.1]);
200         xlabel('Real($\omega$)'); ylabel('Imag($\omega$)')
201         title('Eigenspectra')
202 
203         % Figure title
204         figTitle = {'Eigenfunction', 'Eigenfunction of conjugate pair'};
205         for i = 1:size(eFunction,2)
206             % Eigenfunction plot
207             figure
208             % v-perturbation plot
209             subplot(1,3,1)
210             plot(abs(eFunction(1:end/3,i)),ymesh,'k','Linewidth',1.5)
211             hold on
212             plot(real(eFunction(1:end/3,i)),ymesh,'b--','Linewidth',1.5)
213             plot(imag(eFunction(1:end/3,i)),ymesh,'r--','Linewidth',1.5)
214             legend('Abs($\omega$)','Real($\omega$)','Imag($\omega$)')
215             xlabel('$\tilde{v}$')
216             ylabel('$y$')
217             grid minor; box on; set(gca,'Fontsize',25)
218             title('$\tilde{v}$-Perturbation Profile')
219 
220             % eta-perturbation plot
221             subplot(1,3,2)
222             plot(abs(eFunction(end/3+1:2*end/3,i)),ymesh,'k','Linewidth',1.5)
223             hold on
224             plot(real(eFunction(end/3+1:2*end/3,i)),ymesh,'b--','Linewidth',1.5)
225             plot(imag(eFunction(end/3+1:2*end/3,i)),ymesh,'r--','Linewidth',1.5)
226             xlabel('$\tilde{\eta}$')
```

```
            grid minor; box on; set(gca,'Fontsize',25)
            title('$\tilde{\eta}$-Perturbation Profile')

            % b-perturbation plot
            subplot(1,3,3)
            plot(abs(eFunction(2*end/3+1:end,i)),ymesh,'k','Linewidth',1.5)
            hold on
            plot(real(eFunction(2*end/3+1:end,i)),ymesh,'b--','Linewidth',1.5)
            plot(imag(eFunction(2*end/3+1:end,i)),ymesh,'r--','Linewidth',1.5)
            xlabel('$\tilde{b}$')
            grid minor; box on; set(gca,'Fontsize',25)
            title('$\tilde{b}$-Perturbation Profile')
            sgtitle(figTitle(i))
        end

    end

    %------------------------- END OF FUNCTION --------------------------

end
```

C.3.1 MATLAB Secondary Functions

Listing C.3: `inputValidation.m`

```
function [flow,plotFigure,N,alpha,beta,Re,Fh,theta,Sc] =
    inputValidation(flow,plotFigure,N,alpha,beta,Re,Fh,theta,Sc)

    % ==================== INTRODUCTION TO FUNCTION ======================
    %
    % Function to read, validate and display the main parameters inputs
    %
    % INPUTS:
    % ( 1 ) Chosen shear flow ( pCf = 1; pPf = 2 ) [ flow ]
    % ( 2 ) Request whether to produce plots ( Yes = 1; No = 0 ) [ plotFigure ]
    % ( 3 ) Number of Chebyshev grid points [ N ]
    % ( 4 ) Wavenumber ( x-direction ) [ alpha ]
    % ( 5 ) Wavenumber ( z-direction ) [ beta ]
    % ( 6 ) Reynold number [ Re ]
    % ( 7 ) Froude number ( horizontal ) [ Fh ]
    % ( 8 ) Shear/stratification inalignment angle [ theta ] ( degrees )
    %
    % OUTPUTS:
    % Fully validated inputs

    % ------------------------- BEGIN FUNCTION --------------------------

    while ( flow ~= 1 && flow ~= 2 ) % Validating shear flow
```

```
23        disp('ERROR FROM INPUT')
24        disp('Please ensure the chosen shear flow is either 1 (pCf) or 2 (pPf)!')
25        flow = input('Chosen shear flow (pCf or pPf): ');
26    end
27
28    while ( plotFigure ~= 0 && plotFigure ~= 1 ) % Validating request to plot figures
29        disp('ERROR FROM INPUT')
30        disp('Please ensure that plotFigure is either 0 (do not plot) or 1 (plot)')
31        plotFigure = input('Would you like the eigenspectra/eigenfunction to be
              plotted: ');
32    end
33
34    while ( N ~= round(N) || N <= 2 ) % Validating grid points
35        disp('ERROR FROM INPUT')
36        disp('Please ensure the number of grid points is an appropriate value!')
37        N = input('Number of grid points: ');
38    end
39
40    while ( alpha < 0 ) % Validating wave number (x-dir)
41        disp('ERROR FROM INPUT')
42        disp('Please ensure the chosen wave number (x-dir) is an appropriate value!')
43        alpha = input('Chosen wave number (x-dir): ');
44    end
45
46    while ( beta < 0 ) % Validating wave number (z-dir)
47        disp('ERROR FROM INPUT')
48        disp('Please ensure the chosen wave number (z-dir) is an appropriate value!')
49        beta = input('Chosen wave number (z-dir): ');
50    end
51
52    while ( Re <= 0 ) % Validating Reynolds number
53        disp('ERROR FROM INPUT')
54        disp('Please ensure the chosen Reynolds number is an appropriate value!')
55        Re = input('Chosen Reynold number: ');
56    end
57
58    while ( Fh <= 0 ) % Validating Froude number
59        disp('ERROR FROM INPUT')
60        disp('Please ensure the chosen Froude number is an appropriate value!')
61        Fh = input('Chosen Froude number: ');
62    end
63
64    while ( Sc <= 0 ) % Validating Schmidt number
65        disp('ERROR FROM INPUT')
66        disp('Please ensure the chosen Schmidt number is an appropriate value!')
67        Sc = input('Chosen Schmidt number: ');
68    end
69
```

```
70      % Theta requires no validation
71
72      % Displaying value to user
73      disp('User Inputs: ')
74
75      switch flow
76          case 1
77              fprintf(1, '%s: %s \n', 'flow', 'plane Couette flow')
78          case 2
79              fprintf(1, '%s: %s \n', 'flow', 'plane Poiseuille flow')
80      end
81
82      switch plotFigure
83          case 0
84              fprintf(1, '%s: %s \n', 'plotFigure', 'Eigenspectra/Eigenfunctions will not
                    be plotted')
85          case 1
86              fprintf(1, '%s: %s \n', 'plotFigure', 'Eigenspectra/Eigenfunctions to be
                    plotted')
87      end
88
89      fprintf(1, '%s: %d \n', 'N', N)
90      fprintf(1, '%s: %.3f \n', 'alpha', alpha)
91      fprintf(1, '%s: %.3f \n', 'beta', beta)
92      fprintf(1, '%s: %.3f \n', 'Re', Re)
93      fprintf(1, '%s: %.3f \n', 'Fh', Fh)
94      fprintf(1, '%s: %.3f %s \n', 'theta', theta, 'degrees')
95      disp(' ')
96      disp('Constant parameter:')
97      fprintf(1, '%s: %.3f \n', 'Sc', Sc)
98
99      %-------------------------- END OF FUNCTION --------------------------
100
101 end
```

Listing C.4: `shearFlow.m`

```
1   function [U,DU,DDU,ymesh] = shearFlow(flow,N)
2
3       % ==================== INTRODUCTION TO FUNCTION ======================
4       %
5       % Function to determine velocity profile of chosen the shear flow
6       % Plots of the velocity and stratification profile are also displayed
7       %
8       % INPUTS:
9       % ( 1 ) Chosen shear flow [ flow ]
10      % ( 2 ) Number of Chebyshev grid points [ N ]
11      %
```

```
12      % OUTPUTS:
13      % ( 1 ) Velocity profile [ U ]
14      % ( 2 ) Velocity gradient profile [ DU ]
15      % ( 3 ) Second derivative of velocity profile [ DDU ]
16      % ( 4 ) Domain grid points between -1 to 1 [ ymesh ]
17
18      % ------------------------- BEGIN FUNCTION --------------------------
19
20      % Grid points
21      y = sin(pi*(N-1:-2:1-N)'/(2*(N-1))); % Compute Chebyshev points
22      ymesh = y(2:N-1); % Ignoring boundary points
23
24      % Shear flow either pCf or pPf
25      % User may add other shear flows by adding further cases
26      switch flow
27          case 1 % pCf
28
29              % pCf velocity profiles
30              U = diag(ymesh);
31              DU = eye(N-2,N-2);
32              DDU = zeros(N-2,N-2);
33
34              % Displaying velocity and stratification profile to user
35              disp(' ')
36              disp('Velocity profile: Density profile:')
37              disp('(x,y) plane (X,Y) plane ')
38
39              v_pCf = pCf_plot; % Plot of velocity and stratified profile
40
41          case 2 % pPf
42
43              % pPf velocity profiles
44              U = diag(1 - ymesh.^2);
45              DU = diag(-2*ymesh);
46              DDU = -2*eye(N-2,N-2);
47
48              % Displaying velocity and stratification profile to user
49              disp(' ')
50              disp('Velocity profile: Density profile:')
51              disp('(x,y) plane (X,Y) plane ')
52
53              v_pPf = pPf_plot; % Plot of velocity and stratified profile
54
55      end
56
57      % Functions to plot of velocity and stratified profile
58      % Profiles are hard coded - do not edit these functions
59
```

```
60      % pCf plot
61      function v_pCf = pCf_plot
62
63              % Command window plot
64              v_pCf = char(ones(12,55));
65              v_pCf(:) = ' ';
66
67              for i = 1:6
68                  v_pCf(i,11:22-(2*i)) = '-';
69                  v_pCf(i,22-((2*i)-1)) = '>';
70              end
71
72              for i = 7:11
73                  v_pCf(i,22-((2*i-2))) = '<';
74                  v_pCf(i,11-2*(i-7):10) = '-';
75              end
76
77              for i = 1:11
78                  v_pCf(i,33:32 + 2*i) = '-';
79                  v_pCf(i,32 + 2*i) = '>';
80              end
81
82              % Walls
83              v_pCf(1,1:19) = '=';
84              v_pCf(12,1:19) = '=';
85              v_pCf(1,20:21) = ' ';
86
87              v_pCf(1,33:54) = '=';
88              v_pCf(12,33:54) = '=';
89
90              % Final plot
91              disp(v_pCf);
92
93      end
94
95      % pPf plot
96      function v_pPf = pPf_plot
97
98              % Command window plot
99              v_pPf = char(ones(12,55));
100             v_pPf(:) = ' ';
101
102             % Parabola profile
103             v_pPf(2,9) = '>';
104             v_pPf(3,13) = '>';
105             v_pPf(4,17) = '>';
106             v_pPf(5,19) = '>';
107             v_pPf(6,20) = '>';
```

```
108
109             for i = 2:6
110                for j = 1:20
111                    if ( v_pPf(i,j) == '>')
112                        break
113                    else
114                         v_pPf(i,j) = '-';
115                    end
116                end
117             end
118
119             % Parabolic symmetry
120             for i = 7:11
121                 v_pPf(i,:) = v_pPf(13-i,:);
122             end
123
124             for i = 1:11
125                 v_pPf(i,33:32 + 2*i) = '-';
126                 v_pPf(i,32 + 2*i) = '>';
127             end
128
129             % Walls
130             v_pPf(1,1:20) = '=';
131             v_pPf(12,1:20) = '=';
132
133             v_pPf(1,33:54) = '=';
134             v_pPf(12,33:54) = '=';
135
136             % Final plot
137             disp(v_pPf);
138
139     end
140
141     %-------------------------- END OF FUNCTION --------------------------
142
143 end
```

Listing C.5: `eigenSort.m`

```
1  function eValueSort = eigenSort(eValue)
2
3      % ==================== INTRODUCTION TO FUNCTION ======================
4      %
5      % Function to sort eigenvalues in terms of decreasing imaginary part
6      % Sorted in increasing stablity of eigenmodes
7      %
8      % INPUTS:
9      % ( 1 ) Unsorted eigenvalues [ eValue ]
```

```
    %
    % OUTPUTS:
    % ( 1 ) Fully sorted eigenvalues [ eValueSort ]

    % -------------------------- BEGIN FUNCTION --------------------------

    % sorting e/values in terms of imaginary part
    [~, sortCounter] = sort(imag(eValue));

    % sorted e/values in increasing imaginary part
    eValueSort = eValue(sortCounter);

    % sorted e/values in decreasing imaginary part (more negative)
    eValueSort = flip(eValueSort);

    %-------------------------- END OF FUNCTION --------------------------

end
```

Listing C.6: `chebdif.m`

```
function [x, DM] = chebdif(N, M)

% The function [x, DM] = chebdif(N,M) computes the differentiation
% matrices D1, D2, ..., DM on Chebyshev nodes.
%
% Input:
% N: Size of differentiation matrix.
% M: Number of derivatives required (integer).
% Note: 0 < M <= N-1.
%
% Output:
% DM: DM(1:N,1:N,ell) contains ell-th derivative matrix, ell=1..M.
%
% The code implements two strategies for enhanced
% accuracy suggested by W. Don and S. Solomonoff in
% SIAM J. Sci. Comp. Vol. 6, pp. 1253--1268 (1994).
% The two strategies are (a) the use of trigonometric
% identities to avoid the computation of differences
% x(k)-x(j) and (b) the use of the "flipping trick"
% which is necessary since sin t can be computed to high
% relative precision when t is small whereas sin (pi-t) cannot.
% Note added May 2003: It may, in fact, be slightly better not to
% implement the strategies (a) and (b). Please consult the following
% paper for details: "Spectral Differencing with a Twist", by
% R. Baltensperger and M.R. Trummer, to appear in SIAM J. Sci. Comp.

% J.A.C. Weideman, S.C. Reddy 1998. Help notes modified by
```

```
% JACW, May 2003.

     I = eye(N); % Identity matrix.
     L = logical(I); % Logical identity matrix.

    n1 = floor(N/2); n2 = ceil(N/2); % Indices used for flipping trick.

     k = [0:N-1]'; % Compute theta vector.
    th = k*pi/(N-1);

     x = sin(pi*[N-1:-2:1-N]'/(2*(N-1))); % Compute Chebyshev points.

     T = repmat(th/2,1,N);
    DX = 2*sin(T'+T).*sin(T'-T); % Trigonometric identity.
    DX = [DX(1:n1,:); -flipud(fliplr(DX(1:n2,:)))]; % Flipping trick.
    DX(L) = ones(N,1); % Put 1's on the main diagonal of DX.

     C = toeplitz((-1).^k); % C is the matrix with
     C(1,:) = C(1,:)*2; C(N,:) = C(N,:)*2; % entries c(k)/c(j)
     C(:,1) = C(:,1)/2; C(:,N) = C(:,N)/2;

     Z = 1./DX; % Z contains entries 1/(x(k)-x(j))
     Z(L) = zeros(N,1); % with zeros on the diagonal.

     D = eye(N); % D contains diff. matrices.

    for ell = 1:M
            D = ell*Z.*(C.*repmat(diag(D),1,N) - D); % Off-diagonals
            D(L) = -sum(D'); % Correct main diagonal of D
            DM(:,:,ell) = D; % Store current D in DM
    end
```

Listing C.7: `cheb4c.m`

```
function [x, D4] = cheb4c(N)

% The function [x, D4] = cheb4c(N) computes the fourth
% derivative matrix on Chebyshev interior points, incorporating
% the clamped boundary conditions u(1)=u'(1)=u(-1)=u'(-1)=0.
%
% Input:
% N: N-2 = Order of differentiation matrix.
% (The interpolant has degree N+1.)
%
% Output:
% x: Interior Chebyshev points (vector of length N-2)
% D4: Fourth derivative matrix (size (N-2)x(N-2))
%
```

```
% The code implements two strategies for enhanced
% accuracy suggested by W. Don and S. Solomonoff in
% SIAM J. Sci. Comp. Vol. 6, pp. 1253--1268 (1994).
% The two strategies are (a) the use of trigonometric
% identities to avoid the computation of differences
% x(k)-x(j) and (b) the use of the "flipping trick"
% which is necessary since sin t can be computed to high
% relative precision when t is small whereas sin (pi-t) cannot.

% J.A.C. Weideman, S.C. Reddy 1998.

    I = eye(N-2); % Identity matrix.
    L = logical(I); % Logical identity matrix.

   n1 = floor(N/2-1); % n1, n2 are indices used
   n2 = ceil(N/2-1); % for the flipping trick.

    k = [1:N-2]'; % Compute theta vector.
   th = k*pi/(N-1);

    x = sin(pi*[N-3:-2:3-N]'/(2*(N-1))); % Compute interior Chebyshev points.

    s = [sin(th(1:n1)); flipud(sin(th(1:n2)))]; % s = sin(theta)

alpha = s.^4; % Compute weight function
beta1 = -4*s.^2.*x./alpha; % and its derivatives.
beta2 = 4*(3*x.^2-1)./alpha;
beta3 = 24*x./alpha;
beta4 = 24./alpha;
    B = [beta1'; beta2'; beta3'; beta4'];

    T = repmat(th/2,1,N-2);
   DX = 2*sin(T'+T).*sin(T'-T); % Trigonometric identity
   DX = [DX(1:n1,:); -flipud(fliplr(DX(1:n2,:)))]; % Flipping trick.
DX(L) = ones(N-2,1); % Put 1's on the main diagonal of DX.

   ss = s.^2.*(-1).^k; % Compute the matrix with entries
    S = ss(:,ones(1,N-2)); % c(k)/c(j)
    C = S./S';

    Z = 1./DX; % Z contains entries 1/(x(k)-x(j)).
 Z(L) = zeros(size(x)); % with zeros on the diagonal.

    X = Z'; % X is same as Z', but with
 X(L) = []; % diagonal entries removed.
    X = reshape(X,N-3,N-2);

    Y = ones(N-3,N-2); % Initialize Y and D vectors.
```

```
    D = eye(N-2); % Y contains matrix of cumulative sums,
                                % D scaled differentiation matrices.
for ell = 1:4
         Y = cumsum([B(ell,:); ell*Y(1:N-3,:).*X]); % Recursion for diagonals
         D = ell*Z.*(C.*repmat(diag(D),1,N-2)-D); % Off-diagonal
      D(L) = Y(N-2,:); % Correct the diagonal
DM(:,:,ell) = D; % Store D in DM
end

   D4 = DM(:,:,4); % Extract fourth derivative matrix
```

C.4 Chebyshev Grid Point Convergence

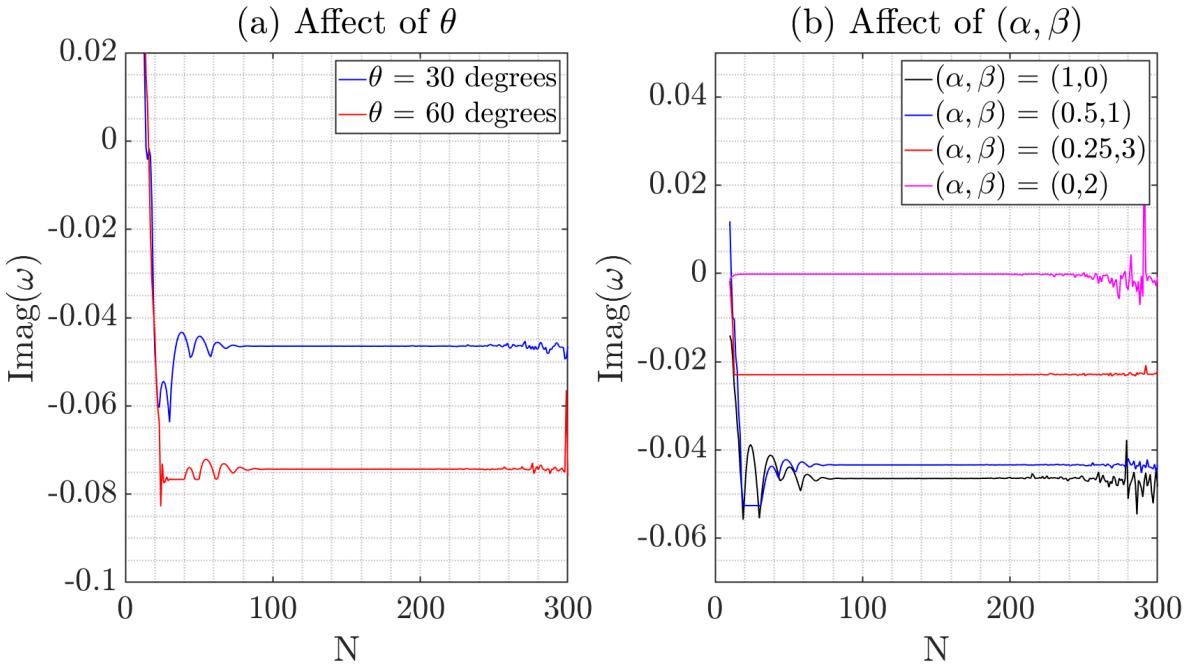

Figure C.4: Convergence of ω_i with varying N for the pCf base profile, where (a) represents different tilt angles and (b) has a variety of wavenumbers.

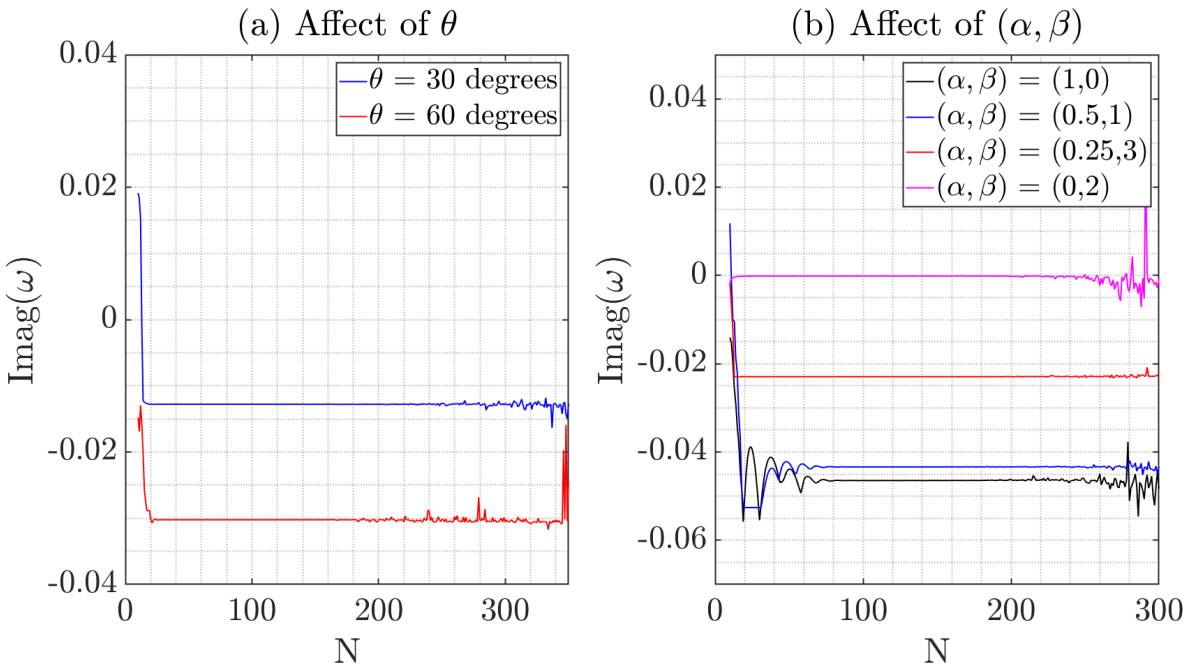

Figure C.5: Convergence of ω_i with varying N for the pPf base profile, where (a) represents different tilt angles and (b) has a variety of wavenumbers.

C.5 Full Validation

Further validation of the Stratified Solver was performed. Due to its supplementary nature, it is presented here to reinforce the accuracy of the developed solver. The comparison between the eigenfunctions is illustrated here.

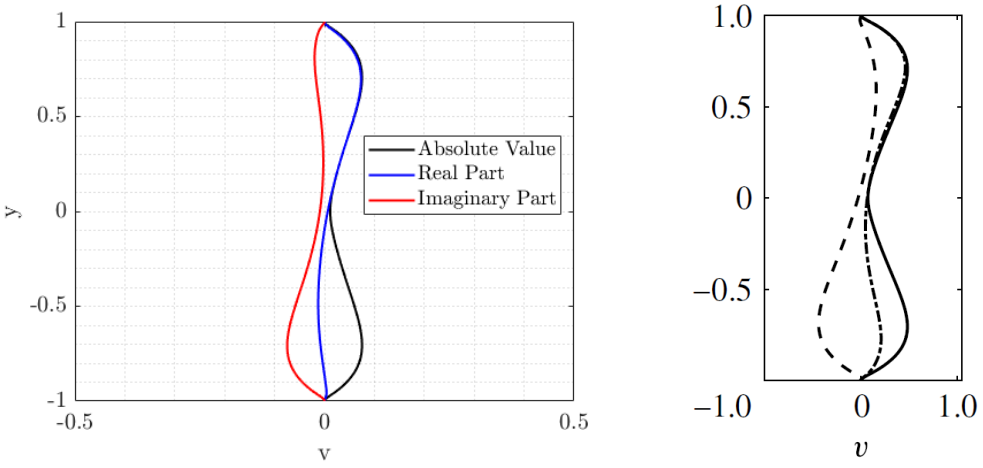

(a) Result from `OS_SQ_Stratified_Solver.m`. (b) Result from Facchini.

Figure C.6: Eigenfunctions of the most unstable eigenmode showing the vertical velocity field, where (a) shows the Solver result and (b) from Facchini [1]. Note that in (b) the solid line refers to the absolute value, dashed-dotted line the imaginary part and the dashed line the real part.

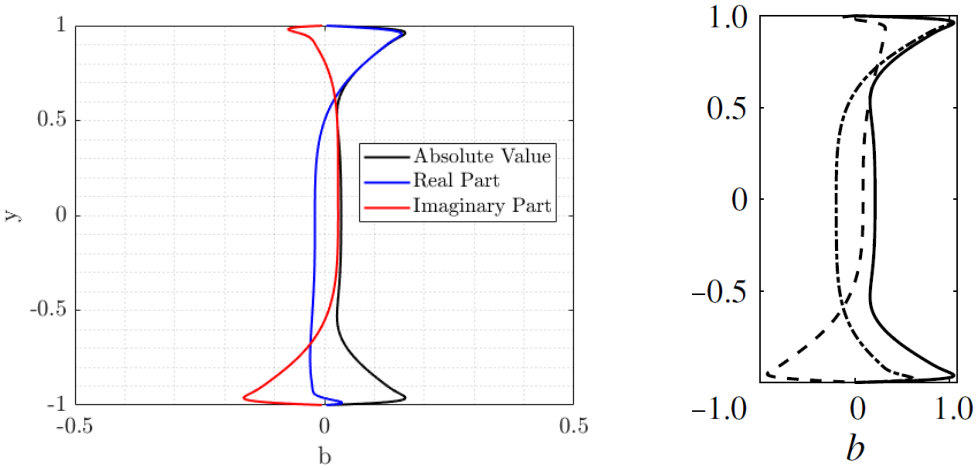

(a) Result from `OS_SQ_Stratified_Solver.m`.

(b) Result from Facchini.

Figure C.7: Eigenfunctions of the most unstable eigenmode showing the buoyancy perturbation, where (a) shows the Solver result and (b) from Facchini [1]. Note that in (b) the solid line refers to the absolute value, dashed-dotted line the imaginary part and the dashed line the real part.

Appendix D

Plane Poiseuille Flow Analysis

In this chapter, the remaining Figures of the pPf, which were not analysed, are included. The main reason being that they followed the same trend as the pCf. The Figures are presented for completeness and to allow deeper analysis of the findings.

D.1 Growth Rate Against Reynolds Number

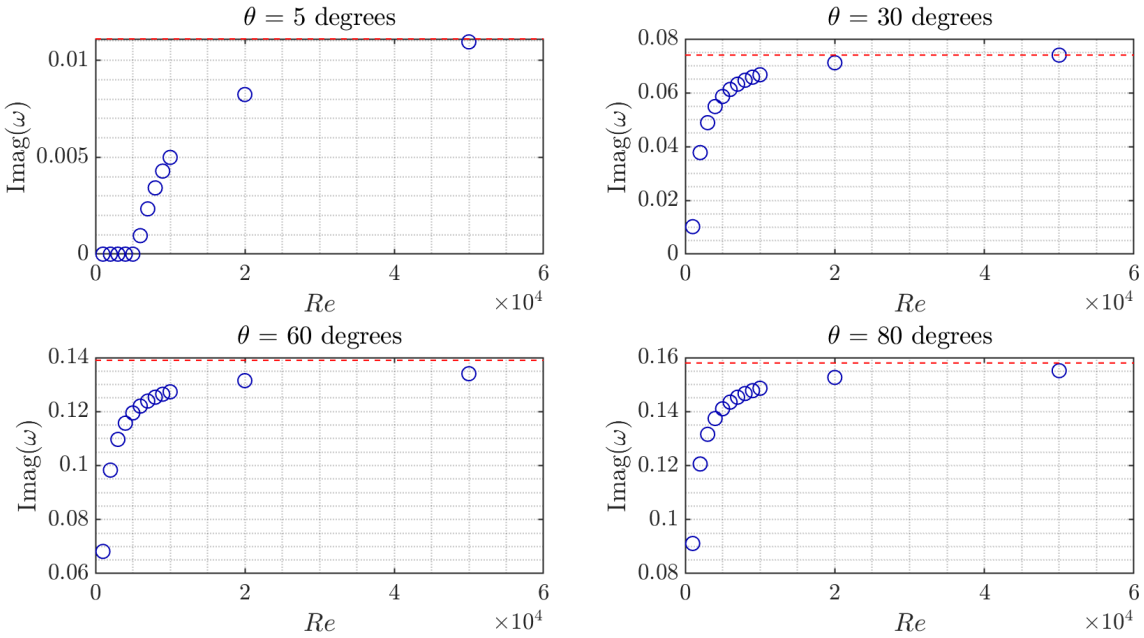

Figure D.1: Growth rate, ω_i, of the most unstable mode as a function of Re with $(\alpha, \beta, F_h) = (1.5, 6, 0.4)$ and θ = (a) 5, (b) 30, (c) 60 and (d) 80 degrees.The red dotted line represents the inviscid solution in the limit $Re \to \infty$.

D.2 Growth Rate Against Inalignment

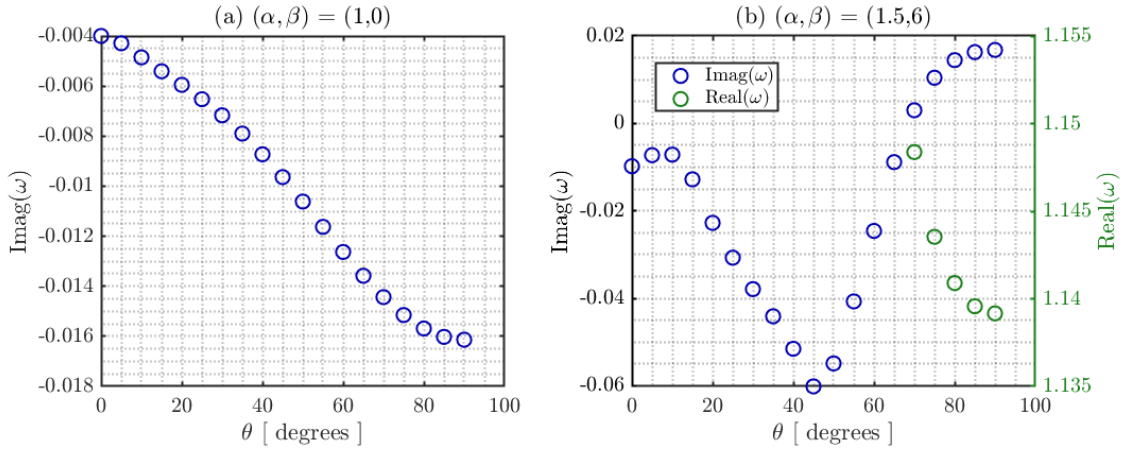

Figure D.2: Growth rate against the tilt angle for inputs $(Re, F_h) = (10000, 1)$ and (α, β) = (a) (1, 0) and (b) (1.5, 6). (b) The oscillatory frequency, ω_r, is plotted for the unstable modes found at the high tilt angles. These values are plotted in green and are with respect to the right green axis.

D.3 Eigenfunction

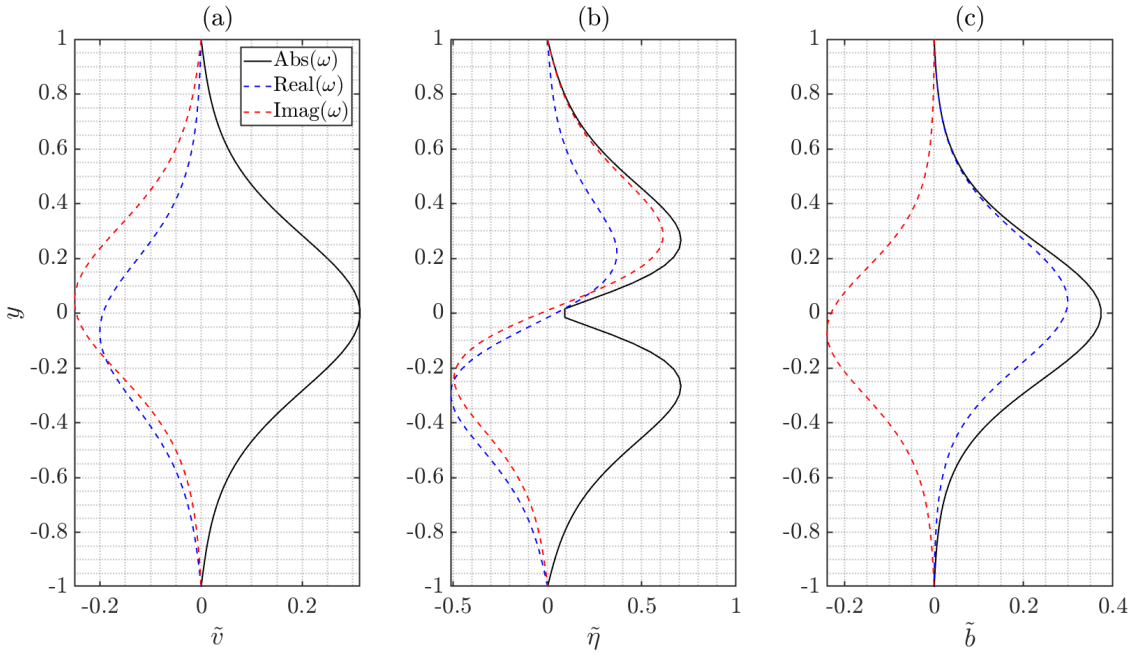

Figure D.3: Eigenfunctions of the most unstable eigenmode with input parameters $(\alpha, \beta, Re, F_h, \theta) = (1.5, 6, 80000, 1, 5)$ for the pPf, where (a) represents the velocity perturbations, (b) wall-normal vorticity perturbations and (c) buoyancy perturbations. Curves refer to the absolute value and real and imaginary parts of ω.

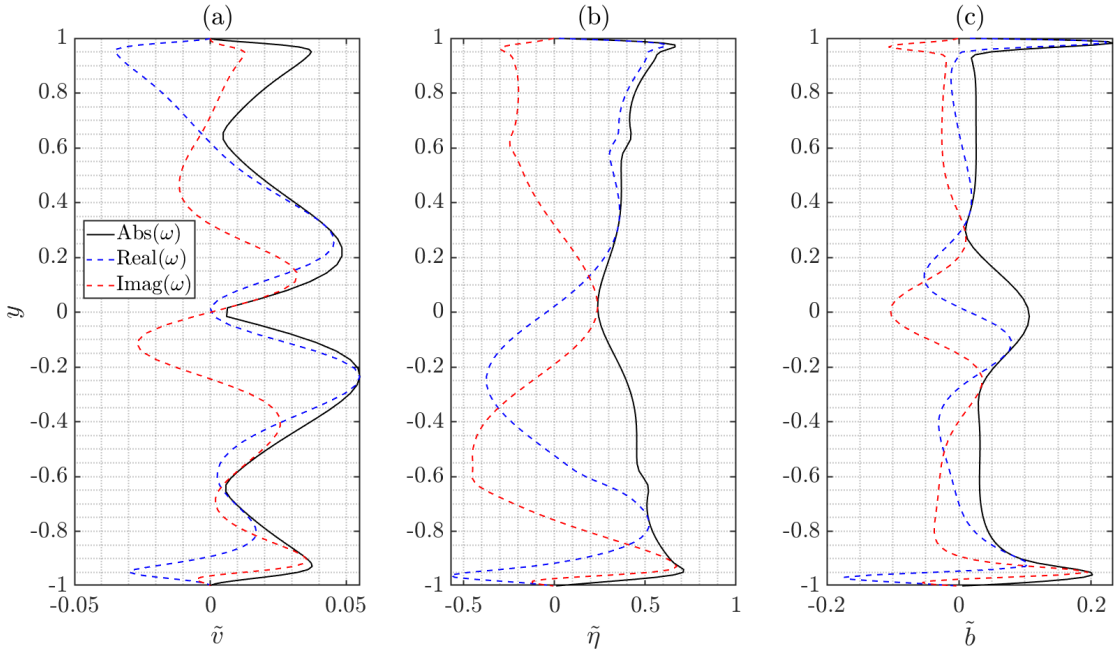

Figure D.4: Eigenfunctions of the most unstable eigenmode with input parameters $(\alpha, \beta, Re, F_h, \theta) = (1.5, 6, 80000, 1, 60)$ for the pPf, where (a) represents the velocity perturbations, (b) wall-normal vorticity perturbations and (c) buoyancy perturbations. Curves refer to the absolute value and real and imaginary parts of ω.

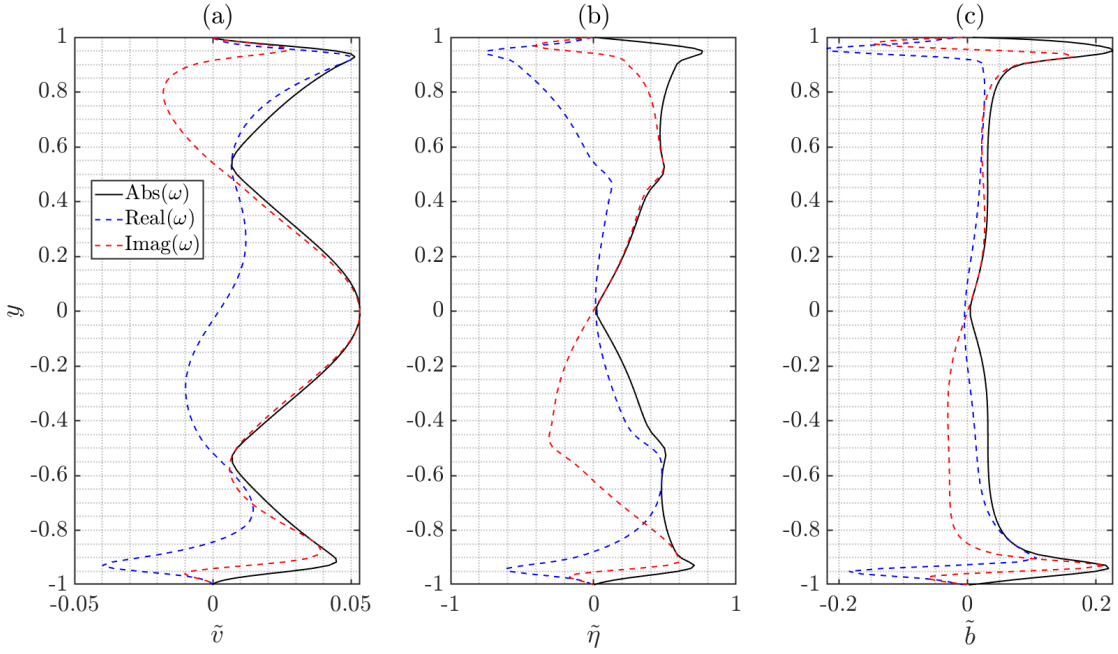

Figure D.5: Eigenfunctions of the most unstable eigenmode with input parameters $(\alpha, \beta, Re, F_h, \theta) = (1.5, 6, 80000, 1, 80)$ for the pPf, where (a) represents the velocity perturbations, (b) wall-normal vorticity perturbations and (c) buoyancy perturbations. Curves refer to the absolute value and real and imaginary parts of ω.